Tuneable Separation in Deterministic Lateral Displacement Devices

Jason P. Beech

Licentiate Thesis
2009

LUND
UNIVERSITY

Division of Solid State Physics
Department of Physics
Lund University, Sweden

Tuneable Separation in Deterministic Lateral Displacement Devices

Printed in Sweden by Media-Tryck, Lund 2009

Division of Solid State Physics
Department of Physics
Lund University
BOX 118
SE-221 00 Lund
Sweden

Abstract

This Licentiate thesis is concerned with particle separation science. More specifically it is concerned with the development of tools for the separation of biologically relevant particles using techniques that have been made possible through the advent of microfluidics. Deterministic lateral displacement, DLD, is a technique that caught our attention because of its exceptional resolution, its suitability for biological separations, the wide range of sizes across which it works and not least because of the promise it holds as a candidate for integration within the miniaturized chemical and biological laboratories that have gained much recent attention and that go under the names micro-total-analysis systems, μTAS, or Lab-on-a-Chip. However, the DLD devices first reported had static separation properties, meaning that they could not be changed without the designing and fabricating of new devices. It also meant that the ability of devices to deal with the dynamic conditions common in biology was limited. Furthermore, the first DLD devices were used for the separation of particles by size only.

The central tenet of this work is that DLD can be used to separate particles by other factors as well as size, for example shape, elasticity or inner structure and that devices that can do this in a tuneable manner will constitute powerful particle separation tools well suited for integration in a Lab-on-a-Chip.

The aim of this Licentiate thesis is to present two research papers, documenting the development of two new methods that improve the existing DLD technique. The first paper describes how the elastomeric properties of poly(dimethylsiloxane) can be utilized to achieve tuneable separation in DLD devices and the second paper presents the use of dielectrophoresis to achieve tuneability, improve dynamic range and open up for the separation of particles with regard to factors other than size.

Throughout this thesis there is talk of cells and other biological particles and yet the papers themselves present separations performed on plastic beads. It is my hope that this initial work is seen in the greater context of our continued research, and as the first step towards putting these new methods to use.

Preface

At some time in the autumn of 2004 shortly after I began work on my diploma project my supervisor, Jonas Tegenfeldt, and I were sitting on a train bound for the Danish Technical University and a meeting with some European Union project partners. Jonas had recently returned from post-doctoral studies at Princeton in the group of Robert Austin and wanted me to do something with a new particle separation method that his lab mates had been working on, but we weren't exactly sure what. Spurred on by the imminent meeting, the discussion was a lively one and by the time we arrived in Denmark we had envisioned much of the work presented here. That it has taken this long to bring the projects to fruition is no reflection of any lack of enthusiasm on my part or on that of Jonas, but is in fact quite the opposite (as the list of related publications bears witness). I would like to thank you Jonas for your part in keeping the spirit of that first meeting alive and for making it possible for me to continue to work on many fascinating projects.

I would also like to thank the members past and present of that migratory band of biophysicists that operate under the codename, "the bio group". Peter Jönsson, without whom paper II would never have got finished, I am so grateful to you that I might actually let you beat me at pool one day, and Fredrik Höök without whom I wouldn't have a job, if you need your basement tiling again I'll see if I can get Nelly to give you a good price. The rest of the group, Magnus, Rodolphe, Brian, Anders, Lisa, Lars-Henrik, Christelle, Waldemar, Gudrun when I see you, you will have to settle for a warm embrace and maybe a pint (Henrik, you will get two pints for proof-reading this).

There are many others at the Solid State Physics department whose help I would like to acknowledge or whom I would like to thank for some small favour or other, from those that toil to keep the money rolling in to those that keep the free coffee flowing, but you are far too numerous to mention by name and so I thank you collectively. There are a few people though that I have bothered slightly more than all the others and whom I would like to thank personally, Mariusz Graczyk, Bengt Bengtsson and Mona Hammar.

Last but not least, Nelly, Jonatan and Freja.

Jason P. Beech
Lund, August 2009

List of publications

This thesis is based on the following papers, which will be referred to by their roman numerals in the text. All material from papers I and II is reproduced by permission of The Royal Society of Chemistry.

I. **Tuneable Separation in Elastomeric Microfluidic Devices**

Jason P. Beech, and Jonas O. Tegenfeldt

Lab Chip, **8**, 657-659 (2008)

My contribution: The project was conceived together with my supervisor Jonas Tegenfeldt. I designed and built the setup and devices, performed the experiments, analyzed the data and wrote the paper.

II. **Tipping the Balance with Dielectrophoresis – Electrical Deterministic Lateral Displacement Devices.**

Jason P. Beech, Peter Jönsson, and Jonas O. Tegenfeldt

Lab Chip, **9**, 2698-2706 (2009)

My contribution: Also conceived together with Jonas. I planned and performed all of the experiments, and wrote most of the paper excluding those parts relating to simulation and modelling which where written together with Peter. Modelling and simulations where performed by Peter. Peter also wrote the particle tracking software.

Related publications

The following related publications by the author are not included in the thesis.

III. Use of PLL-g-PEG in Microfluidic Devices for Localising Selective and Specific Protein Binding

Rodolphe Marie, **Jason P. Beech**, Janos Vörös, Jonas O. Tegenfeldt, and Fredrik Höök

Langmuir, **22**, 24, 10103-10108 (2006)

IV. Nanoconfinement-enhanced Conformational Response of Single DNA Molecules to Changes in Ionic Environment

Walter Reisner, **Jason P. Beech**, Niels B. Larsen, Henrik Flyvbjerg, Anders Kristensen, and Jonas O. Tegenfeldt

Physical Review Letters, **99**, 5, 058302 (2007)

V. Multidirectional Sorting Modes in Deterministic Lateral Displacement Devices

Brian R. Long, Martin Heller, **Jason P. Beech**, Heiner Linke, Henrik Bruus and Jonas O. Tegenfeldt.

Physical Review E, Stat Nonlin Soft Matter Phys**, 78**, 11, 146304 (2008)

VI. Shear-Driven Motion of Supported Lipid Bilayers in Microfluidic Channels

Peter Jönsson, **Jason P. Beech**, Jonas O. Tegenfeldt, and Fredrik Höök

J. Am. Chem. Soc. **131**, 14, 5294-5297 (2009)

VII. The Mechanical Behavior of a Supported Lipid Bilayer under External Shear Forces

Peter Jönsson, **Jason P. Beech**, Jonas O. Tegenfeldt, and Fredrik Höök

Langmuir, **25**, 11, 6279-6286 (2009)

Contents

1 Introduction

As particle-laden fluids are forced to flow through channels containing ordered arrays of micrometer-sized obstacles the particles follow paths through the arrays that are highly dependent on both the size and layout of the array and on the size of the particles themselves. A technique exploiting this behaviour to separate particles by size was reported by Huang *et al.* in 2004 [1], and was given the name Deterministic Lateral Displacement, DLD. Huang showed how the resolution in these devices could be much greater than in conventional size-based separation techniques, reporting a resolution of 10nm when separating micrometer sized polymer beads, an order of magnitude improvement compared to hydrodynamic chromatography. Subsequent work has shown how DLD can be used for the separation and analysis of various biological particles [2-5] in devices no larger than a centimetre or two in size.

This introductory chapter will deal with some of the terms used in the above paragraph. It will explain what biological particles are, why one might want to separate them from one another, how the methods for doing this differ from one another and why performing particle-particle separations in miniaturised devices is so attractive and the focus of much current research.

1.1 Particles

The word particle probably conjures up a variety of images for you depending on your background. You might think of an elementary particle, such as a proton, or something more tangible, like a particle of sand. The word particle comes from the Latin, *particula* meaning 'little part' and is therefore equally suited to both protons, atoms, molecules and pieces of sand despite a span in mass of 20 orders of magnitude. Much of the work performed in research laboratories and in industrial processes involves the breaking down of complex mixtures into their constituent parts (or particles) and the subsequent separation of these particles from one another. Whether it is the breaking down of a sample of soil into size sorted particular fractions or the breaking down of just one of these soil particles into its constituent atoms the processes used come under the rubric, separation science [2].

Particle	Diameter (μm)
Whole cells:	
Bacterial	0.5-5.0
Yeast	2.0-10
Fungi and algae	40-70
Mammalian cells	5-40
Plant	50-100
Cell debris:	
Bacterial	0.05-3.0
Yeast	0.05-8.0
Inclusion bodies†	0.05-1.2
Crystals	1.0-100
Virus and Virus-like particles‡	0.02-0.2
† Aggregates, usually of proteins that are the result of viral activity	
‡ VLP:s are virus capsids without nucleic acid contents.	

Table 1.1. An overview of bioparticle sizes [3].

1.2 Separation of Biological Particles

Biological particles are for example the constituent parts of biological systems or the results of biotechnological processes and range in size and complexity from individual molecules such as proteins to single cells and even entire (micro)organisms. A wide variety of techniques with which particles in the relevant size range, see table 1.1, can be separated has been developed, each with its inherent advantages and disadvantages [7, 8]. Particles in the range 20μm to 10mm have been separated using sieves, 0.1μm to 1mm with membrane filtration, 1μm to 150μm with elutriation and split flow thin fractionation and the smallest particles, 10nm to 10μm, are often separated using Capillary Electrophoresis. These techniques have all been used for the separation of biological particles. Flow cytometry is a method widely used for the sorting of cells [4] and flow cytometers ranging in size from desktop models to room sized are standard pieces of equipment at most large hospitals. While flow cytometers can sort cells at rates of up to 100 000† per second they are expensive and require extensive infrastructure such as lab space, power, personnel and reagents as discussed by Pappas and Wang [5]. Although information about the size and granularity of particles can be gleaned from scattered light, generally these methods also require the fluorescent labelling of samples. While these requirements are

† For example, Accuri C6 Flow Cytometer® 10 000 detection events s^{-1} and BD FACSAria™ 70 000 detection events s^{-1}.

easily met in large hospitals they can be a limiting factor in other settings from laboratories to developing-world health clinics. Another drawback of large flow cytometers is that they are not suited to integration with other analysis steps, something that is crucial to fully benefit from the opportunities offered by microfluidics.

1.3 The advent of μTAS and Lab-on-a-Chip

In 1979 Steven Terry used techniques borrowed from the electronics industry‡ to fabricate a gas chromatograph on a silicon wafer that despite being three orders of magnitude smaller than its conventional laboratory predecessors suffered no loss of function [6]. In 1990 Manz proposed the integration of modules with the capabilities of performing all the steps necessary for the chemical analysis of a biological sample on a single chip [7]. In the last 20 years much work has been done on the development of these micro total analysis systems or μTAS. 'Lab-on-a-chip' is a slightly broader term encompassing the miniaturization of any chemical or biological process to chip scales that has also become widespread and we will use this term throughout the thesis to denote such miniaturized systems. The benefits of this miniaturization and integration are many including increased automation, parallelization, speed and resolution and portability as described in reviews by Dittrich and Manz [14], Franke and Wixforth [8], Erickson [9], Verpoorte [10] and Craighead [11]. Several other reviews have covered the progress made towards chips that can be used in Cellomics research [12-14] in which microfluidics techniques are used to solve the problems specific to the field and in which multiple steps such as cell sorting, cell trapping, cell lysis and contents analysis can be performed.

The goal for many researchers in the fields of μTAS and Lab-on-a-chip is at present the development of devices that will be able to diagnose a patient at the bedside in just a few minutes without the need for extensive laboratory testing. These so called point-of-care, or POC, diagnostic devices, it is believed, stand to revolutionize the health care industry, not least in the developing world as proposed by Yager in Nature [15] due to their low cost and portability, and will help to usher in an era of personalized medicine in which treatments are tailored to the individual based on richer and more

‡ The group of techniques developed to fabricate integrated circuits, such as photolithography to define patterns and etching to transfer those patterns into a material, typically silicon, are collectively known as "micromachining". A comprehensive catalogue of techniques developed to date can be found in Marc Madou's Fundamentals of Microfabrication and Nanotechnology [Madou, M. J., *Fundamentals of Microfabrcation and Nanotechnology* 3rd ed. 2009, Boca Raton: CRC Press. 2640 p.]

frequently collected diagnostic data taken from increasingly smaller samples.

Because many biologically relevant samples such as whole blood, saliva and cell lysates are highly complex and because the targets for detection can be present in extremely low concentrations, separation is often an essential part of any analytical process. The problem in theses cases is basically analogous to that of the classic needle in a haystack. The job of separation is to remove as much of the hay as possible before one begins hunting for the needle. Separation or pre-concentration can be necessary at more than one stage in a process as described by Chen and Cui [13]. For example if cells are being analyzed then it might be necessary to first isolate the cells of interest. These cells can then be lysed after which further separation of the proteins or genetic material in the cell lysate can be performed. Because of the importance of separation there has been great focus on both the miniaturization of the traditional methods of particle separation mentioned above and on the development of new techniques based on phenomena that emerge at the microscale, such as low Reynolds number flows.

In order for separation and the closely related pre-concentration techniques to be integrable within a Lab-on-a-chip it is advantageous, as described by Pamme [16], that the process be continuous. Continuous methods differ from batch methods in which separation is performed on finite volumes of sample in a serial manner. Batch methods can be integrated with other analysis steps but require controlled sample injection and flow switching for the collection of separated fractions that greatly increase the complexity of devices. Continuous methods accept the input of a sample at one end, separate the particles in space, and allow for the extraction of any number of fractions at the other. The continuity of flow through such devices means that they can be more easily integrated with other analysis steps both upstream and downstream.

1.4 Deterministic Lateral Displacement

DLD is a method of particle separation that is, in light of the discussions above, well suited for the separation of biologically relevant particles (the mechanism of DLD will be described in chapter 4). In the first paper by Huang *et al.* [1], DLD is presented as a purely size-based separation technique with an exceptional resolution of down to 20nm in diameter when separating micrometer sized polystyrene beads. The method is deterministic in nature meaning that unlike many other separation techniques it does not rely on stochastic processes like diffusion that need to be given time to work and can therefore be run arbitrarily fast, provided the criteria for low Reynolds number flow are met as will also be discussed in the following

chapters. This means that volume flow rates of ~ml/min can be achieved in a single device. Higher throughputs could be achieved by the running of many devices in parallel[†].

DLD has proven capable of dealing with biological samples. The technique has so far been used to separate chromosomal bacterial DNA of differing lengths [1], red and white blood cells together with platelets and plasma in various combinations [17] and healthy and malignant lymphocytes [18]. DLD has also been used to detect changes in the hydrodynamic size distribution of blood platelets due to the effects of thrombin and refrigeration [19]. The size range of particles that have been separated in DLD devices span from 100's of nanometers [20] to tens of micrometers [2-5, 25-27] meaning that they are capable of dealing with both whole cells and their constituent parts. Because particles are caused to move across streamlines in a DLD device they can be moved through laminar flow streams containing different chemistries. Morton *et al.* used this fact to lyse cells, stain the nucleus upon release and subsequently separate the stained nucleus from the unwanted debris [21]. As well as separation the ability of DLD to steer streams of particles independently of flow can be used to focus or disperse these streams [22].

Being continuous, DLD has all the advantages that such methods have to offer. As discussed above, this makes DLD ideally suited for integration with other components in a Lab-on-a-Chip. Continuity is also important in the context of tuneable separation devices, the focus of our present work, as will become apparent in the following chapter.

1.5 Tuneable Deterministic Lateral Displacement Devices

Papers I and II, presented in this thesis, deal with the development of DLD devices (see Fig. 1.1) that are both tuneable and able to separate particles with respect to parameters other than size. Despite the proven power of DLD to make high-resolution separations over a wide range of particle sizes, the critical sizes in those devices reported in the literature have been fixed. This means that devices must be designed and fabricated to fit the particles one wishes to separate based on prior knowledge of their hydrodynamic radii. However, the hydrodynamic radius of the particles in

[†] We previously presented a method of hot embossing DLD devices in thin films. Many of these thin devices could be stacked in order to achieve throughput [Beech, J.P., et al., *Throughput Through Thin-Film Fluidics.* 12th International Conference on Miniaturized Systems for Chemistry and Life Sciences, 2008: p. 1492-1494].

the system of interest may not be known. The radii of particles may change over time. Cells for example grow or change size and conformation due to experimental conditions. Soft particles may be deformed by interactions with carrier fluids and obstacles, which will change their effective radii, and non-spherical particles may behave differently depending on their orientation as they move through the device. *Tuneability*, together with continuity, makes it possible to perform separations with live feedback, where for example image analysis is used to evaluate the results of a separation and the running parameters are adjusted accordingly in order to reach the desired outcome at each given point in time. This can be a powerful tool in the analysis of biological systems that are in their nature extremely dynamic.

Paper I describes how we have used the elastomeric properties of poly(dimethylsiloxane) to change the geometry of the post array in a DLD device during ongoing separation therefore achieving tuneable, size-based separation.

Paper II describes how forces can be added to DLD in order to achieve tuneability with regards not only to size but also to other particle properties. In the specific case reported in Paper II we use the application of electric fields that give rise to dielectrophoretic forces within the post array to achieve tuneability. These DEP forces are sensitive not only to particle size but also to the dielectric characteristics of particles which can be leveraged to separate cells, for example, live from dead, healthy from sick or cells at different stages of their developmental cycle that might not display any significant differences in size.

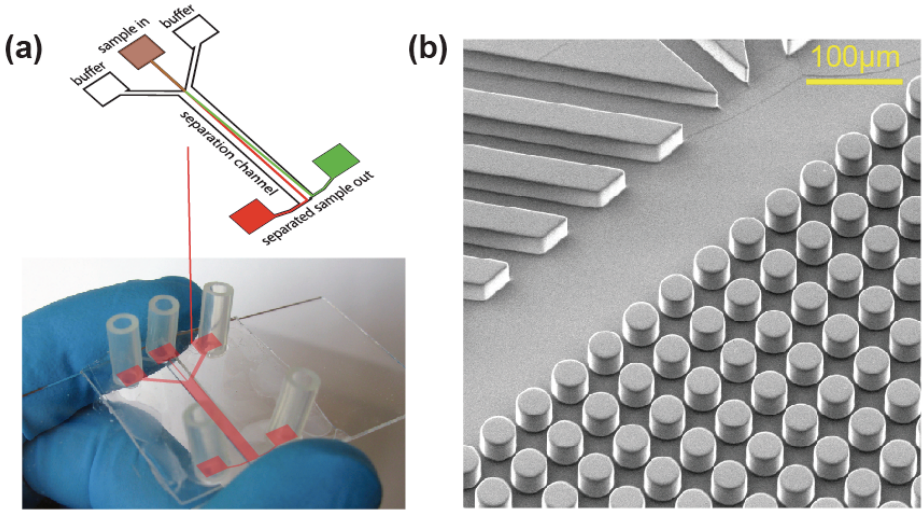

Figure 1.1. DLD devices fabricated in PDMS. (a) A typical device for stretching experiments with the channel structures highlighted in red (b) A scanning electron micrograph taken at the entrance to the post array. The straight structures to the left are channels that ensure a focused stream of the particles that are to be separated. The distance between these elastomeric posts can be changed by the application of stress. Alternatively their insulating properties can be used to deform an electric field.

The devices described in papers I and II are continuous, tuneable, able to deal with both biological and nonbiological samples, can separate particles in the range 100nm to 100µm and are therefore of great interest both as stand-alone separation devices and as integrable components for Lab-on-a-Chip.

2 Microfluidics

Definition of a fluid: *A fluid is a substance that continually deforms under the action of shear stress.*

We are all familiar with fluidics on the macro scale. A jet of water from a garden hose, the bubbling and gurgling of a running stream or the swirling of your morning coffee as you stir in the sugar are everyday examples of fluids behaving under the influence of applied forces. Fluids are caused to move by body forces such as gravity, normal forces such as pressure and shear forces that give rise to viscosity. We learn about these forces and how to balance them when we learn to swim. With the exception of extremely slow moving fluids (see Fig 2.1a), inertial effects dominate fluid flow on the macro scale (see Fig 2.1b). The situation is very different for fluids flowing through the micrometer scale environments encountered within the field of microfluidics. On these scales inertia is almost always negligible and behaviour is dominated by viscous forces, by surface effects such as surface tension and wetting and by diffusion and can sometimes seem counterintuitive or at the least unfamiliar to the uninitiated. This chapter will briefly introduce some of the concepts most central to microfluidics with the focus on those phenomena that underlie the workings of deterministic lateral displacement devices.

The interested reader is referred to the books by Bruus [23], Hauke [24], Nguyen and Wereley [25] for derivations and in-depth discussions of the physics of microfluidics and also to several review papers [14, 15, 22, 31-35].

2.1 The Navier-Stokes Equation

Newton's second law states that the net force on an object is equal to the mass of that object multiplied by its acceleration.

$$\mathbf{F} = m\mathbf{a} \tag{1}$$

While a raindrop can be seen as an object and while Newton's second law is capable of describing the motion of its centre of mass, the detailed behaviour of the liquid within the raindrop requires a description of the fluid as a continuous medium rather than as a discrete mass. Instead of discrete forces and masses fluids can be described in terms of continuous

fields such as density (mass) and force density. The Navier-Stokes equation describes the velocity field in a Newtonian fluid†.

$$\rho\left[\frac{\partial \mathbf{v}}{\partial t} + (\mathbf{v}\cdot\nabla)\mathbf{v}\right] = -\nabla p + \eta\nabla^2\mathbf{v} + \mathbf{f} \tag{2}$$

$$\nabla\cdot\mathbf{v} = 0 \tag{3}$$

Eq. 2 is analogous to Newton's second law with inertial acceleration terms to the left and force terms on the right. ρ is the density, $\mathbf{v}$ the velocity, p the pressure, η is the dynamic viscosity and $\mathbf{f}$ represents body force densities such as those arising from gravity and electrical forces.

Eq. 3 is the continuity equation, arrived at by assuming an incompressible fluid where ρ is constant in both time and space.

2.2 The Reynolds Number and the Stokes Equation

Because of the nonlinear term in the Navier-Stokes equation it cannot generally be solved analytically. Luckily, the equation can be greatly simplified under specific conditions such as those found at the small length scales relevant for microfluidic devices. Because it is the inertial term $(\mathbf{v}\cdot\nabla)\mathbf{v}$ that causes the problem we want to know when it can be neglected. If we consider a flow of fluid in the x-direction with a velocity gradient in the y-direction, the viscous force acting on an area A in the xz-plane is

$$F_{viscous} = \eta A\frac{dv}{dy} \sim \eta l^2\frac{v}{l} = \eta l v \tag{4}$$

The inertial effects can be estimated as

$$F_{inertial} = ma \sim \rho l^3\frac{v^2}{l} = \rho l^2 v^2. \tag{5}$$

The ratio between equations 4 and 5 can be written

$$\frac{F_{inertial}}{F_{viscous}} = \frac{\rho l v}{\eta} \equiv \mathrm{Re}, \tag{6}$$

† For Newtonian fluids the viscosity η is assumed not to vary.

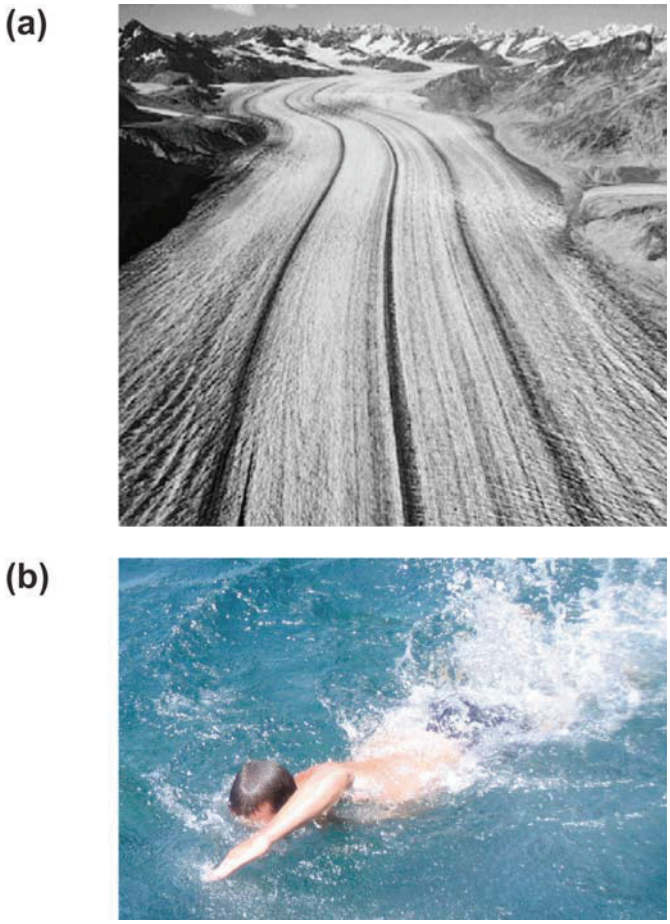

Figure 2.1. Laminar or turbulent flow? (a) Due to the high viscosity, flow in a glacier is laminar. Streamlines move parallel to one other and turbulence is absent. Copyright Wiley-VCH Verlag GmbH & Co. KGaA. Reproduced with permission [8]. (b) The author investigating inertial effects and turbulence at the macro scale.

In Eq. 4 the length l is the side of the area element over which the viscous drag force occurs and in Eq. 5 it is the radius of curvature about which the fluid flow changes direction and is in both cases a length that characterizes the system†. Re is a dimensionless number known as the Reynolds number

† The characteristic length is often taken to be the smallest length scale of the system such as the radius for a particle or the smallest width of a channel. The hydraulic diameter D_H for a channel is also commonly used:

$$D_H = \frac{4 \times \text{cross sectional area}}{\text{wetted perimeter}}$$

after Osborne Reynolds. The Reynolds number is ubiquitously used to predict if and when the Navier-Stokes equation can be simplified. Systems with large spatial dimensions, high densities, large velocities or small viscosities are characterized by large Reynolds numbers (see Fig 2.1b). It is such flow, known generally as turbulent flow that we are well acquainted with on the macro scale. The flow of coffee around the inside of a cup is dominated by inertia (stop stirring and see what happens) and is therefore in general turbulent, exhibiting eddies and vortices that are characteristic of turbulent flow. The onset of turbulence depends on the geometry of the system and occurs only when inertia totally dominates, becoming increasingly more likely for Re>1500. For Reynolds numbers spanning the range on the order 1 to 1000, non-turbulent inertial effects such as Dean flow and non-turbulent vortices may occur. Low Reynolds numbers characterize systems with sufficiently small dimensions, low densities, low velocities or high viscosities (see Fig 2.1a). In microfluidic systems with water as the fluid, characteristic channel dimensions in the range 10^{-6} m to 10^{-3} m and characteristic velocities in the range 10^{-6} m s^{-1} to 10^{-3} m s^{-1} *Re* ranges from 10^{-6} to 1 and viscosity dominates. Under such conditions when the inertial terms can be neglected the Navier-Stokes equation simplifies to the linear Stokes equation,

$$0 = -\nabla p + \eta \nabla^2 \mathbf{v} \tag{7}$$

2.3 Laminar Flow

Laminar flow is essential in order for DLD to function. The word lamina means, “thin layer”, and laminar means, “consisting of thin layers”. In fluidics these thin layers consist of non-mixing parallel flows, often visualised by particles or dye molecules. Such laminae can be seen in the glacier shown in Fig. 2.1a, and Fig. 2.3 shows laminar flow in a microchannel. Fig 2.2 shows a simulation of pressure driven flow through an array of posts performed in COMSOL Multiphysics® 3.4 (COMSOL AB, Stockholm, Sweden) using the Stokes equation (Eq, 7). The array has the same dimensions as that used in Paper II.

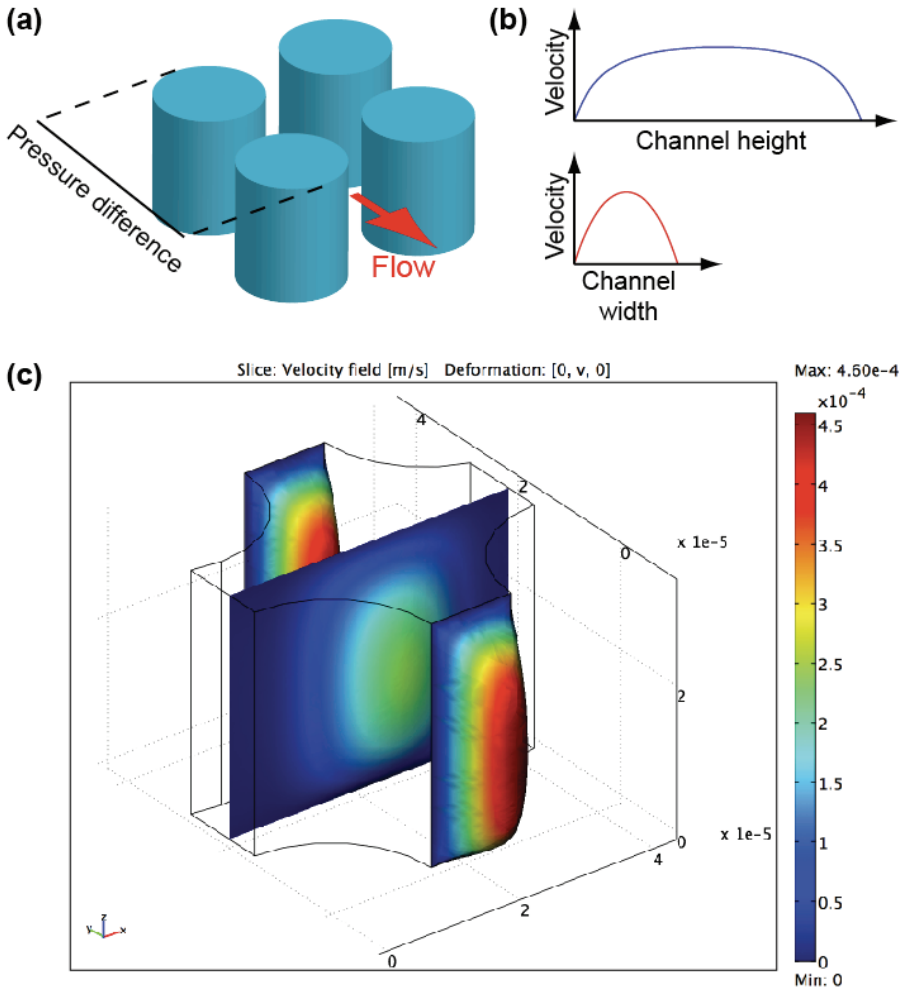

Figure 2.2. Calculating flow profiles in post arrays (a) Flow is generated through a post array using a pressure difference. (b) Solving the Stokes equation gives the velocity profile between the posts. For the smallest dimension, the gap between the posts, the profile is close to parabolic. (c) Simulated flow through a post array with the same dimensions as that used in Paper II performed using COMSOL Multiphysics® 3.4 (COMSOL AB, Stockholm, Sweden) using the Stokes equation (Eq, 7). The velocity profile is shown with a colour coded scale ranging from 0 μm s^{-1} to 450 μm s^{-1}. The flow is driven by a pressure drop of 12 Pa mm^{-1} and with the smallest dimension 12μm and the maximum flow rate 450 μm s^{-1} the Reynolds number is ~0.005.

The Reynolds number is in this case $Re=\rho vl/\eta=10^{3}\cdot 450^{-6}\cdot 12\cdot 10^{-6}/10^{-3}\sim 0.005$ and the flow exhibits all the characteristics of laminar flow.

If two fluids are flowing in two channels that meet in a "Y" geometry, provided the flow is characterised by low *Re,* the two fluids will continue to flow next to each other as if they are still confined by channel walls as can be seen in Fig. 2.3. In the absence of any applied forces, the only transport between laminae is due to diffusion as will be described in section 3.4.

Another important feature of laminar flow, which will become important later when we look at the theory of DLD, is the velocity profile. The velocity profile between the posts in the simulation can be seen in Fig 2.2b and Fig. 2.2c. Because of the viscous drag from the walls of the channel the flow velocity is highest in the centre of the channel and lowest towards the wall. This effect is analogous to what happens when you push out the middle of a deck of cards with your finger while holding the top and bottom cards still. The fluid laminae slide across each other in a manner similar to the cards. The velocity field forms a parabola across the width of the channel, the smallest dimension. Across the depth of the channel the profile is parabolic near the wall but flattens out in the centre.

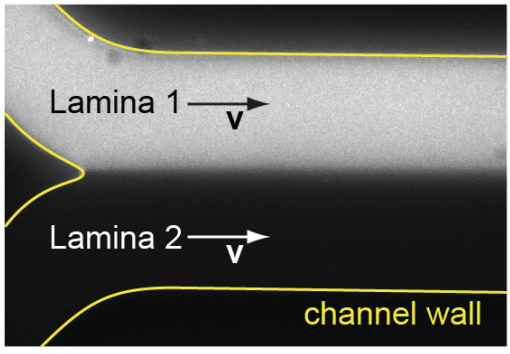

Figure 2.3. Two streams meet but continue as if still confined by channel walls. These non-mixing streams are referred to as lamina and such flow is called laminar flow.

3 Particles in fluid flows

3.1 Viscous drag contra applied forces

A rigid sphere of radius *a* moving with velocity **v**† relative to an incompressible fluid with viscosity η, as depicted in Fig 3.1, will at low *Re* experience a viscous drag force given by Eq. 8.

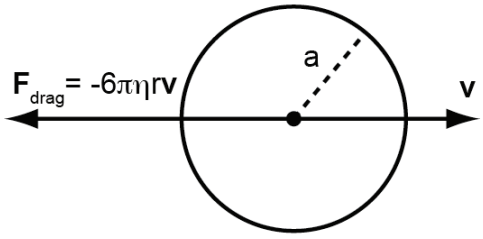

Figure 3.1 Viscous drag on a spherical particle.

$$\mathbf{F}_{drag} = -6\pi\eta r\mathbf{v} \tag{8}$$

This drag force dominates the behaviour of particles at low Reynolds numbers. Consider for example a neutrally buoyant sphere of 1μm radius moving under the influence of a constant force at 100μm s^{-1} in water. When the force is removed the particle will stop within ~0.3 ångström‡. Due to the dependence of the drag force on the velocity, the particle nears this distance in an exponential manner, which would take an infinitely long time. In reality though the motion becomes dominated by collisions with water molecules and within microseconds the particle will, except for this Brownian motion, come to a standstill. What this means is that, although inertial effects have been used for separation even at Reynolds numbers of around one [26, 27], in most cases the inertia of the particle can be neglected. There are two important conclusions to draw from this: Firstly in the absence of forces other than viscous drag, particles move at the same

† The particle velocity **v** is relative to the velocity of the media at distance *d* from the centre of the particle where $d \to \infty$. The no slip boundary condition is given by **v**=0 for *d*=*a*.

‡ $\Delta x = \frac{v_0 m}{6\pi\eta r}\left(1 - e^{-t\frac{6\pi\eta r}{m}}\right)$

velocity as the suspending fluid medium and they will at all times follow streamlines. Secondly, any additional force applied to a particle will cause the particle to accelerate, or to cross streamlines, but will quickly be balanced by viscous drag. A constant force will therefore cause a particle to move with constant velocity.

Fluidics-based particle separation techniques are almost exclusively based on the application of selective forces, dependent on specific particle characteristics, that force particles into streamlines that a) move with differing velocities, leading to separation in time, or b) leave a device at differing positions leading to separation in space.

The forces that cause particles to cross streamlines are numerous and give rise to the wealth of techniques mentioned in the introduction. These forces can be divided into stochastic and deterministic forces. Diffusion is a stochastic process, present to varying degrees in all microfluidics systems. The other forces are deterministic in nature. These are externally applied body forces such as gravity, electrophoretic and dielectrophoretic forces, magnetic forces, acoustic forces and steric forces.

In the following sections we will look at the effects that are important for separation in DLD devices. We will look first at the interaction of particles with channel walls, which we will refer to as steric interactions, which underlie the separation mechanism of DLD. Dielectrophoresis is used in Paper II to tune the behaviour of particles in DLD devices and will also be reviewed briefly. Finally diffusion, always present at the microscale and often working against our efforts to separate particles, will be considered.

Note about effects that we neglect in the current discussion: The polystyrene particles used in our measurements have a density marginally greater than that of water (1050kg m^{-3} as opposed to 1000kg m^{-3} for water), giving them negative buoyancy. This means that due to the influence of gravity they will sink over time. While particles may sediment in reservoirs, where they can spend several hours due to the large volumes and low flow rates, most are too small to sediment on the timescales relevant to transit through a device. We also assume that all effects of DLD discussed in the present work are independent of the position of particles normal to the device plane and we therefore neglect sedimentation. Electrophoresis is due to the action of an electric field on the fixed net charge of a particle. In paper II AC fields are used in which the electric field and thus the electrophoretic force average to zero. Like sedimentation, electrophoresis will not be discussed here.

3.2 Steric hindrance – Clogging and non-clogging filters

Particles can only follow streamlines provided they are physically able to do so. A sieve is based on the fact that particles are unable to follow streamlines through constrictions that are smaller than the particles themselves (see Fig 3.2). A wide variety of devices have been fabricated using constrictions in various geometries [28-30], with the aim of achieving separation. Constrictions have also been used to trap individual cells [31] and droplets containing cultures of cells [32]. These techniques are inherently "clogging", due to the fact that, as is the case with a traditional filter or sieve, particles remain in the sieving structure and will eventually hinder the performance of the separation. Clogging devices are well suited to particle-liquid separation where the removal of all particles is the aim. Inline water filters are a good example of this. They are not however as well suited to particle-particle separations as the effective pore size changes rapidly as soon as particle capture begins.

Non-clogging devices are those that use steric forces from channel walls to force particles to cross streamlines while simultaneously allowing them to flow through the device. Pinched flow [33] is a method that utilizes this effect. DLD is also a non-clogging sieve.

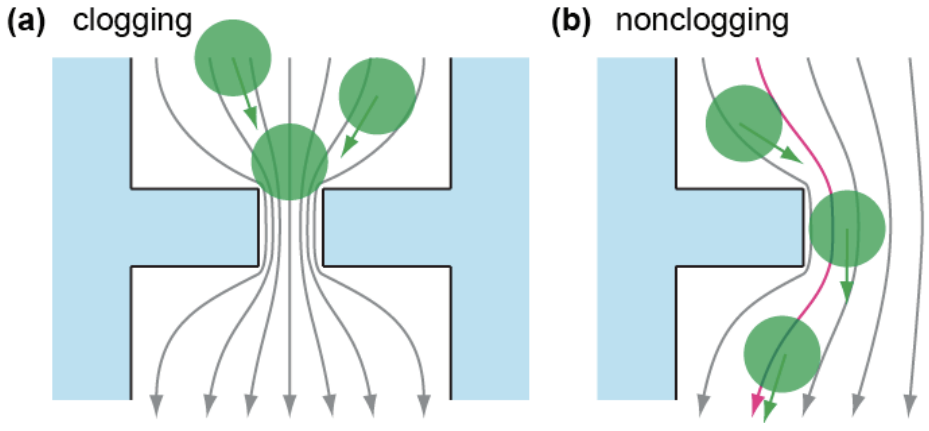

Figure 3.2. Clogging and non-clogging particle separation geometries. (a) In a sieve-like device particles are trapped in constrictions. (b) Non-clogging devices allow particles to move through the device but force them to cross streamlines.

3.3 Dielectrophoresis

DEP is the movement of polarisable particles due to the forces they experience in a non-uniform electric field and was explored in the 1960s by Pohl [34-37]. The dielectrophoretic energy, W_{DEP}, and force, $\boldsymbol{F}_{\mathrm{DEP}}$, on a spherical particle are given by [38]

$$W_{DEP}(x,y,z) = -2\pi\varepsilon_m r^3 \,\mathrm{Re}(f_{CM})\left|E_{RMS}(x,y,z)^2\right| \tag{9}$$

$$\mathbf{F}_{DEP} = -\nabla W_{DEP}(x,y,z) = 2\pi\varepsilon_m r^3 \,\mathrm{Re}(f_{CM})\nabla\left|E_{RMS}(x,y,z)^2\right| \tag{10}$$

where f_{CM} is the Clausius-Mossotti factor:

$$f_{CM} = \frac{\varepsilon_p^* - \varepsilon_m^*}{\varepsilon_p^* + 2\varepsilon_m^*}, \tag{11}$$

$$\varepsilon^* = \varepsilon - j\frac{\sigma}{\omega}. \tag{12}$$

In Eqs. 9 and 10 ε_{m} and ε_{p} are the permittivities of the medium and the particle respectively, r the particle radius and $\boldsymbol{E}_{RMS}$ the root-mean-square value of the electric field. $\varepsilon_{\mathrm{m}}^*$ and $\varepsilon_{\mathrm{p}}^*$ are the complex permittivities as defined by Eqs. 11 and 12 where ε is the permittivity and σ the conductivity of the particle/medium and ω is the angular frequency of the applied field.

We can consider what happens to f_{CM} in the limits where either ε_{m} or ε_{p} go to zero. If the particles are more polarisable than the surrounding medium (see Fig. 3.3a), we let $\varepsilon_{\mathrm{m}}\rightarrow 0$ and we get $f_{CM}=1$. If the opposite is true (see Fig. 3.3b), then $\varepsilon_{\mathrm{p}}\rightarrow 0$ and we get $f_{CM}=-0.5$ so the range of $f_{CM}=[-0.5,1]$. It is the real part of f_{CM} that decides in which direction the DEP force will act. In general, if we have $\mathrm{Re}(f_{CM})>0$ then the potential energy of the particle will have a minimum where the electric field is highest. These particles will be pushed away from regions with a low electric field towards regions with a high electric field. This effect is known as positive DEP (pDEP) (see Fig. 3.3c). If on the other hand $\mathrm{Re}(f_{\mathrm{CM}})<0$ then the potential energy will be largest where the electric field has a maximum resulting in a reversal of the force (see Fig. 3.3d). Force towards areas of low electric field is known as negative DEP (nDEP).

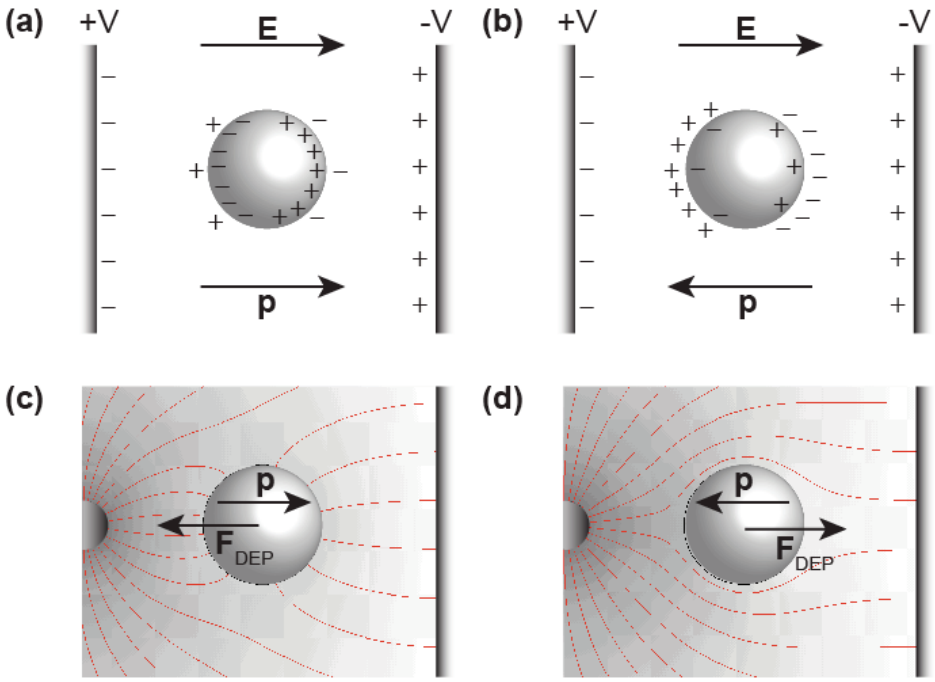

Figure 3.3. Particles become polarised differently depending on the relationship between their polarisability and that of the suspending medium. (a) If a particle is more polarisable than the suspending fluid then more charges build up on the inside of the particle/fluid medium interface and a net dipole, **P**, is induced that is parallel with the electric field. (b) If the particle is less polarisable than the suspending medium then less charge builds up on the inside of the boundary and **P** points in the opposite direction to the field. (c) If a particle more polarisable than the suspending medium is placed in an electric field gradient it will experience a force in the direction of the gradient. This is positive DEP. (d) In the opposite case the particle experiences negative DEP.

Electric field gradients can be generated in two ways, either using the geometries of electrodes or by modifying the field using insulators (see Fig 3.4). These methods will be dealt with in chapter 6.

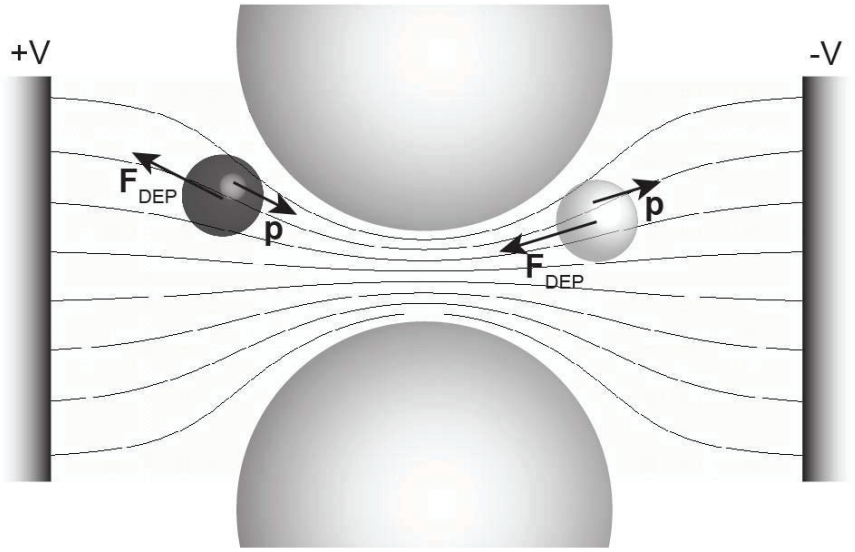

Figure 3.4. Electric field gradients can be created in microfluidic channels using insulating constrictions that squeeze field lines together. The dark particle is experiencing negative DEP and the light particle is experiencing positive DEP.

3.4 Diffusion

For low-Reynolds number flows, mixing is driven by diffusion only. The mean square distance that a particle diffuses in time t is given by:

$$\left\langle x^2 \right\rangle = 2k \cdot Dt \tag{13}$$

where k is the dimensionality of the problem and is equal to 1, 2 and 3 for 1, 2 and 3 dimensional diffusion respectively. D is the diffusion coefficient and is given by the Stokes-Einstein relation.

$$D = \frac{k_B T}{6\pi\eta a} \tag{14}$$

Here k_B is Boltzmann's constant[‡], T the temperature and a the particle radius. Diffusion is omnipresent in microfluidic devices at experimental time scales. Although diffusion has been used to separate particles [28] in the context of DLD it serves only to reduce resolution and must always be considered. The Péclet number expresses the relative importance of convection to diffusion.

[‡] At room temperature $k_B T = 4 \cdot 10^{-21}$ J.

$$\mathrm{Pe} \equiv \frac{\text{diffusion time}}{\text{convection time}} = \frac{V_0 a}{D} \tag{15}$$

Fig 3.5 shows particles of 1μm and 10nm respectively flowing at v=30μm $^{-1}$ in a 10μm wide lamina. The particles have very different diffusion constants and the difference in the effect diffusion has on the two streams of particles is pronounced. Fig 3.5a shows how at high flow rates and therefore high *Pe* the effects of diffusion are relatively small over the length of the channel and the stream remains well defined. The stream of 10nm particles however, characterised by a much smaller *Pe*, becomes greatly broadened. In DLD devices where streams of particles are created it is essential that Péclet numbers are high enough that the streams do not become significantly blurred due to diffusion.

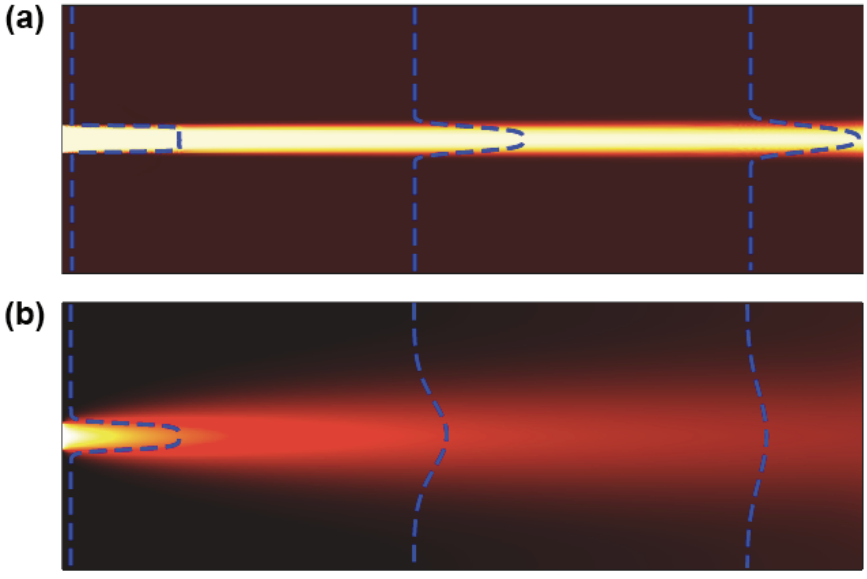

Figure 3.5 Simulation (COMSOL Multiphysics® 3.4 (COMSOL AB, Stockholm, Sweden)) of a 10μm wide stream of particles entering from the left into a channel 100μm by 300μm with an average flow velocity of 30 μm s^{-1}. (a) Particles with a radius of 1μm are characterized by *Pe* = 40 000. The particle stream is only very slightly broadened by diffusion. (b) Particles with a radius of 10nm are instead characterized by *Pe* = 400. During the time taken for the particles to traverse the channel the stream is considerably broadened. The concentration profile in both cases is shown in blue.

4 Deterministic Lateral Displacement

In light of previous discussions we are now ready to consider DLD. DLD devices consist of row-shifted arrays and we will begin this chapter by defining such arrays in section 4.1. As fluid flows through these arrays the flow is bifurcated by the posts and divided into a number of discrete laminae in a process described in section 4.2. This will bring us to the key point, which is how particles behave in such flows. There are two modes of transport for particles carried in such a bifurcated flow; they are either able to remain in one lamina and will follow the fluid flow in the average flow direction, or they are forced by steric interactions with posts to cross streamlines into neighbouring laminae thus having their overall trajectories altered. Particles can then be collected at different positions at the end of the device. This mechanism, which is affectionately known as "bumping", will be described in section 4.3.

4.1 Row-shifted arrays

The post arrays used in DLD devices are periodic. If the average flow direction is defined by sidewalls (see Fig 4.1a) then "Row-shift" refers to the fact that each successive row along the flow direction is shifted by a distance $\Delta\lambda$ perpendicular to the flow direction. If in row number N+1 the posts have the same positions as in row 1 then we say that the array has a period N[†]. There are two ways to achieve this shift, using tilted square arrays and rhombic arrays as shown in Figs 4.1b,c respectively. In Paper I the arrays used were of the rotated square array type whereas those used in Paper II where of the rhombic type. While there may be small differences in these two types of row-shifted arrays, for example with regards to fluid resistance along different directions in the array as discussed by Inglis [39], rhombic arrays are simpler to draw in CAD software and are therefore the type we predominantly use. We therefore confine discussions here to the case of rhombic arrays. For rotated square arrays $\Delta\lambda$ can be calculated as $\lambda\cdot\tan(\theta)$ and the arguments for rhombic arrays are assumed to hold true.

[†] Arrays with non-integer row-shifts are studied in Paper V but are outside the scope of this thesis. As is discussed in this paper non-integer row-shifts give rise to multiple sorting modes. Using sedimentation as a driving force in order to achieve arbitrary row-shifts we have been able to experimentally demonstrate the existence of such modes. (to be presented at the μTAS 2009 conference, South Korea)

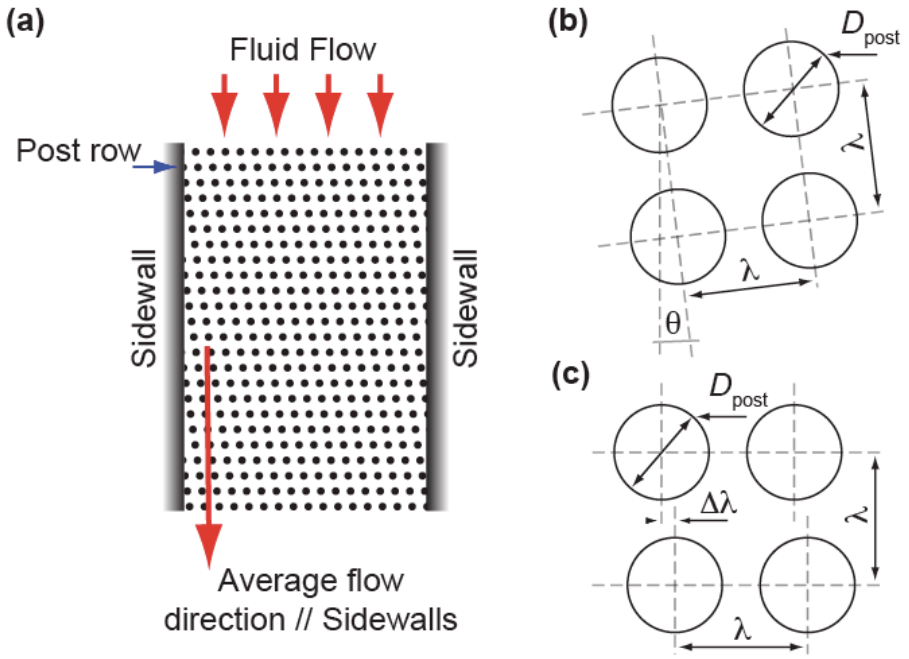

Figure 4.1. Post array geometries. (a) The sidewalls in a device define an average flow direction. (b) A rotated square array as used in Paper I (c) A rhombic array as used in Paper II.

4.2 The Characteristics of Flow Through Row-Shifted Arrays

The total fluid volume flux between two posts in row 1 (see Fig. 4.2a) for an example of an array with N=5, can be defined as Φ_{gap}. Due to the periodicity of the array and the laminarity of the flow, Φ_{gap} can be divided into N laminae, which we will call Φ_i where i=1 to N, where the boundary between each laminae is defined by bifurcations around posts. Each of these laminae carries a volume flux of Φ_{gap}/N and follows a cyclic path through the array as depicted in Fig. 4.2a. The positions at which the laminae pass between the posts are, again due to the laminarity of the flow, well defined and can be numbered P_i also for i=1 to N. As we will see in the next section it is the width of Φ_1 at position P_1 that determines the behaviour of particles and so we need to determine this width.

Figs. 4.2b and 4.2c show the parabolic flow profile between posts. Because the fluid flux in a lamina is conserved, its width depends on its velocity and therefore its position, P_1, P_2, P_3, ..., P_N, in the flow profile. Due to

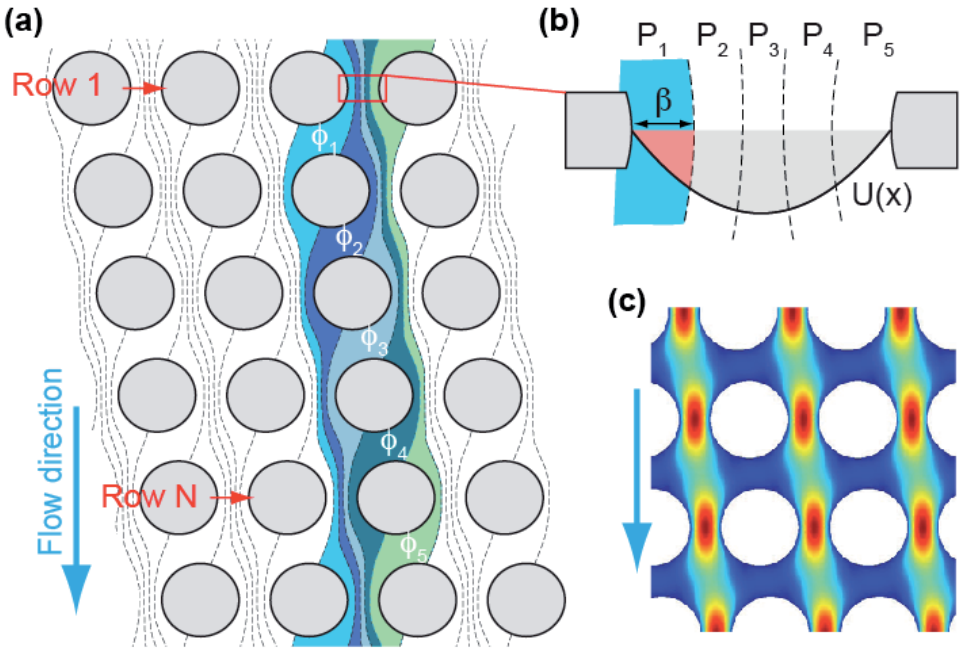

Figure 4.2. Fluid flow through a row-shifted array with a period, N=5. (**a**) The flow becomes bifurcated by the posts and is divided into a series of laminae. Each of the laminae, labeled $\phi_{1,2,\ldots,5}$, moves through the array passing between the posts at 5 well-defined positions, which we number P_1 to P_5. A lamina that passes between two posts in a specific row at P_N will in the subsequent row occupy P_{N-1}. This is repeated until the lamina is back at P_1 after one period, N. (b) The positions P_1 to P_5 that the laminae occupy as they move through the array. Because of the flow profile the laminae have widths that depend on which of the positions they occupy. (c) Finite-element simulation of flow through a post array. The colour map shows the velocity profile with red fast and dark blue slow.

the stick boundary conditions at the surface of the post the fluid velocity is lowest here and the width of the lamina is therefore widest at P_1 and P_N. This width, which we will refer to as β, can be calculated by solving the following integral:

$$\Phi_1 = \frac{1}{N}\,\Phi_{gap}$$

$$\int_0^{\beta} u(x)dx = \frac{1}{N}\int_0^{d} u(x)dx \tag{16}$$

The following derivation is similar to the one presented by Inglis *et al.* [40]. Assuming a parabolic flow profile:

$$u(x) = \left[\frac{d^2}{4} - \left(x - \frac{d}{2}\right)^2\right], \tag{17}$$

where d is the distance between posts and is equal to λ-D_{post}. The solution to the integral is:

$$\beta = \frac{d}{2}\left[1 + 2w + \frac{1}{2w}\right], \tag{18}$$

where

$$w^3 = \frac{1}{8} - \frac{N^{-1}}{4} \pm \sqrt{\frac{N^{-1}}{16}\left(N^{-1} - 1\right)}. \tag{19}$$

The correct root of w^3 is

$$w = \left[\frac{1}{8} - \frac{N^{-1}}{4} \pm \sqrt{\frac{N^{-1}}{16}\left(N^{-1} - 1\right)}\right]^{(1/3)}\left(-\frac{1}{2} - i\frac{\sqrt{3}}{2}\right). \tag{20}$$

For back-of-the-envelope calculations the following approximation† is considerably easier to handle and works well for commonly used periods, N>10:

$$\beta_{approx} = \sqrt{\frac{N}{3}} \cdot \frac{d}{N}. \tag{21}$$

This approximation is arrived at by making the same assumptions as in Eq. 16 but by then assuming that $1/N \approx \beta/d$ (see the second line of the derivation below):

$$\frac{1}{N} = \frac{\int_0^{\beta} \frac{d^2}{4} - \left(x - \frac{d}{2}\right)^2 dx}{\int_0^{d} \frac{d^2}{4} - \left(x - \frac{d}{2}\right)^2 dx} = \frac{\left[\frac{d\beta^2}{2} - \frac{\beta^3}{3}\right]}{\left[\frac{d^3}{2} - \frac{d^3}{3}\right]} = 3\left(\frac{\beta}{d}\right)^2 - 2\left(\frac{\beta}{d}\right)^3 =$$

† This approximation was first presented by Jonas Tegenfeldt during a meeting at MIC/DTU Aug 17 2004, "Bumper Array 17 2004.ppt" Slides #17-22.

$$= \left(\frac{\beta}{d}\right)^2 \left[3 - 2\frac{\beta}{d}\right] \approx \left(\frac{\beta}{d}\right)^2 \left[3 - 2\frac{1}{N}\right] \approx 3\left(\frac{\beta}{d}\right)^2 \Leftrightarrow$$

$$\Leftrightarrow \frac{N}{3} \approx \left(\frac{\beta N}{d}\right)^2 \Leftrightarrow \beta \approx \sqrt{\frac{N}{3}} \cdot \frac{d}{N}$$

Eq. 18 and Eq. 21 are plotted in Fig. 4.4a.

4.3 The Mechanism of Deterministic Lateral Displacement

Now that we have described the flow of fluid through a row-shifted array of posts we can consider what will happen to particles suspended in that fluid. Due to the viscous drag force described in chapter 3.1, particles will follow the fluid flow wherever possible remaining within a lamina but they will also, as was explained in chapter 3.2, interact sterically with posts. The mechanism of DLD can now be explained on the basis of these two effects.

Particles whose hydrodynamic centre of mass† fit into a lamina at P_1 will remain within the lamina and will therefore move through the array in the average flow direction whereas larger particles are displaced by the post into P_2‡. This displacement occurs at every row causing the particles to move at an angle, $\theta = \arctan(\Delta\lambda/\lambda)$, relative to the fluid flow (see Fig 4.3b,c and d). The terminology for these two modes used in Papers I and II reflects the character of their trajectories and is the same as that used by Huang *et al.* [1]: particles that follow the flow move in the *zigzag mode*; deflected particles move in the *displacement mode* (see Fig 4.3b).

In the previous section we derived the width of the lamina at P_1, β, as a function of the array parameters. We can now define the critical size in a DLD device as $D_{c0}=2\beta$. An analytical expression for the critical size is:

$$D_{c0} = 2\alpha\frac{d}{N}. \qquad (22)$$

Here $d = \lambda - D_{post}$ is the inter-post distance and $N = \lambda/\Delta\lambda$, is the period of the array as defined in Fig. 4.1. The unit-less parameter α contains the effects of the flow profile and can be measured using the stretching method

† This is the point in the particle that never crosses lamina (without the influence of applied forces) and is the same as the centre of mass for a hard sphere at low Re.
‡ Displacement into P_i for i>2 will have the same result.

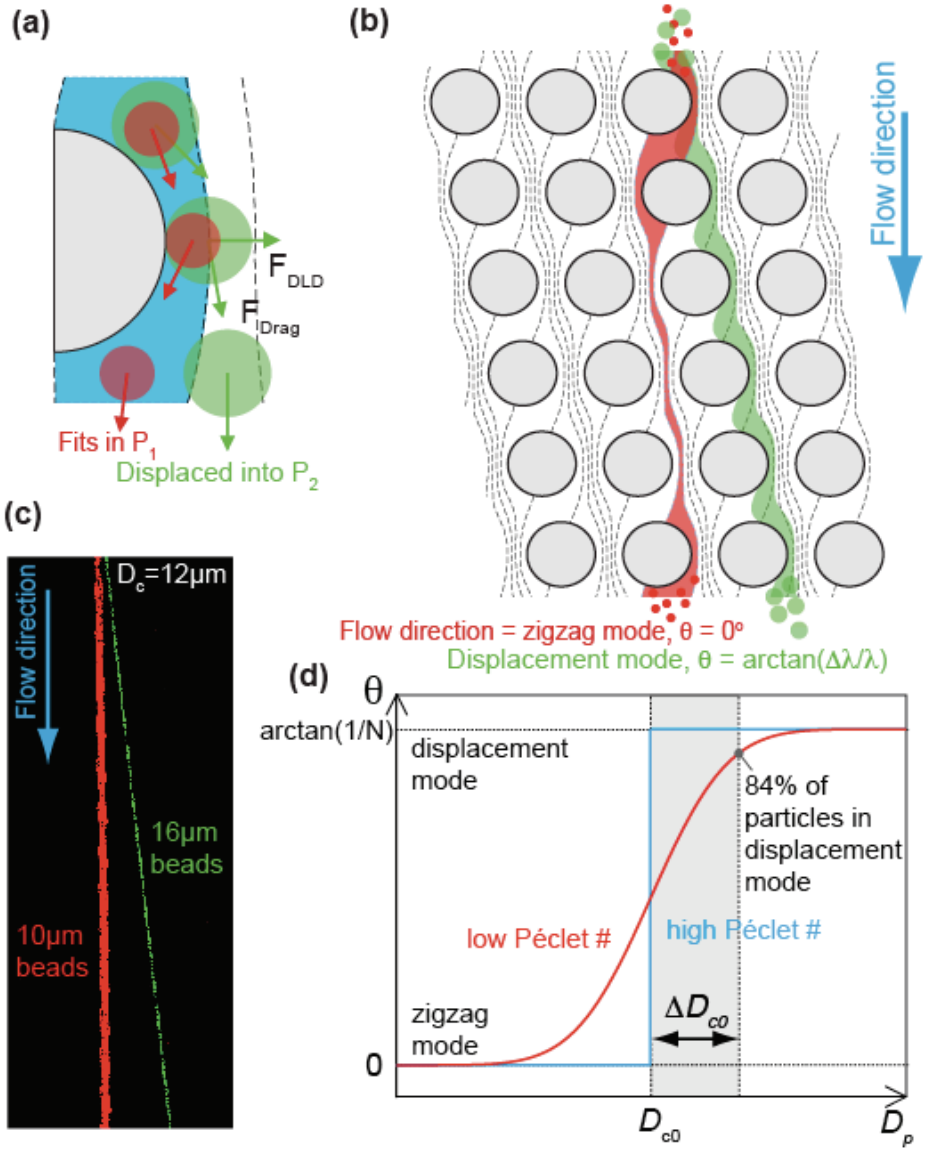

Figure 4.3. The mechanism of separation by DLD. (a) A particle with a hydrodynamic diameter less than D_{c0} is able to remain within the lamina at P_1. A particle with a diameter larger than D_{c0} is forced by the post into the lamina at P_2 in a process affectionately known as "bumping". (b) This "bumping" is repeated at each row leading to separation between the smaller particles that follow the flow direction and the larger particles that follow a direction defined by the row-shift in the array. (c) A colour enhanced micrograph of separation in an actual device. (d) The particle trajectories measured relative to the flow direction as a function of particle diameter, D_p. The transition is broadened by diffusion.

described in the next chapter and in Paper I. Fig. 4.4a shows D_{c0}, normalized to d, as calculated using Eq. 18 (blue), Eq. 21 (red). Fig. 4.4b shows the difference between D_{c0} calculated using Eq. 18 and Eq. 21. For relevant N, that is N>10, the approximation works well. Experimental values taken from Papers I and II are also shown (green crosses).

It is important to note that the theoretical derivation of β shown in Eq. 18 (and the subsequent approximation in Eq. 21) is based on several simplifications and that there are effects that may act to alter the critical size by varying degrees depending on the situation.

Firstly, we have assumed a two-dimensional flow profile. In 3 dimensions the flow profile may deviate near the edges and corners of the channel. For micrometer-sized particles that are unable, due to interactions with the walls, to probe the flow near the wall these effects are negligible. Small particles (~100nm) however may be able to probe these volumes and will be affected. Also, the 2-D flow profile between posts is only parabolic for fully developed flows. The ratio between the post diameter D_{post} and the gap size d will have an effect on the velocity profile. Fig 4.5 shows three profiles for different d/D_{post} ratios. In black it can be seen that for small gap sizes relative to the post size the profile is almost exactly the same as the parabola shown in red. As the ratio d/D_{post} increases the deviation from the parabolic

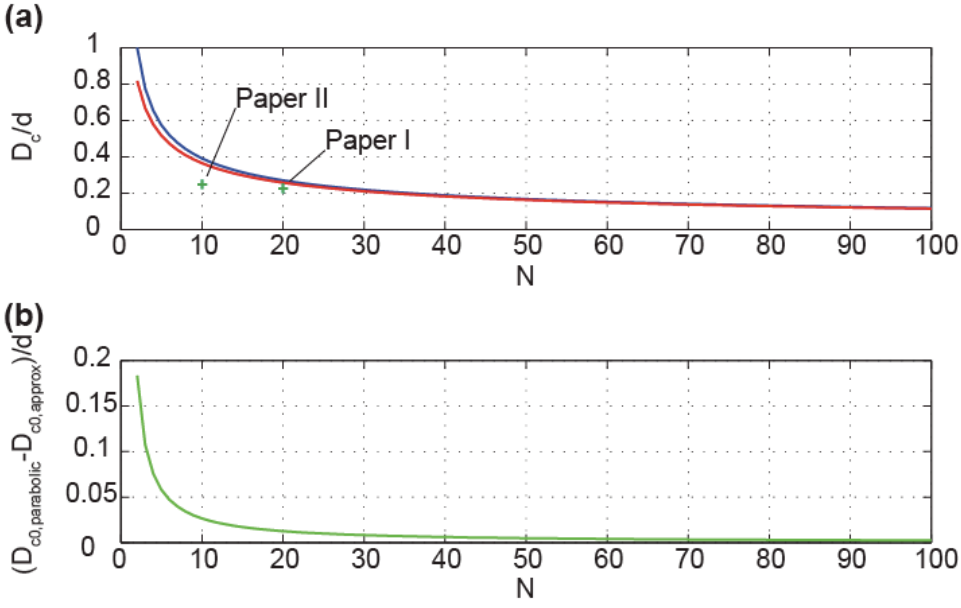

Figure 4.4. Critical size in DLD devices. (a) In blue a plot of D_{c0} (normalized to the inter-post gap d) as a function of the period N in a DLD device calculated as 2β where β is calculated using Eq. 18. In red $D_{c0}=2\beta_{approx}$ where β_{approx} is calculated using Eq. 21. The green crosses show measured values from Papers I and II. (b) The error due to the approximation is small for relevant N, (N>10).

becomes more pronounced. The devices we have used have $d/D_{\text{post}} \leq 1$ and the parabolic profile is a good approximation. The shape of the posts has also been shown to have an effect on the flow profile. Loutherback *et al* used asymmetric posts between which flow profiles are asymmetric to achieve DLD devices in which the critical size depends on whether the flow is in the positive or negative direction [41].

Secondly, the presence of the particles themselves can have a large effect on the fluid velocity field. A particle that is almost as large as d will affect the flow considerably; influencing both its own behaviour and that of nearby particles. This effect is more pronounced for shallow devices than for deep ones.

A third effect is that of diffusion. Fig. 4.3d shows how diffusion broadens the transition between the zigzag and displacement modes. This effect, shown as symmetric about D_{c0} in the figure, actually acts to shift D_{c0} to the left. The shift originates in the fact that diffusion acts differently on particles in the zigzag mode than it does on particles in the displacement mode. For more details of this effect the reader is referred to the discussion by Heller and Bruus [42] and that in Paper V.

From this discussion we conclude that there are many factors that influence D_{c0} in DLD devices and that the theory is still in its infancy. Despite this it is still possible to design devices using the principles we have discussed that will have D_{c0} reasonably close to the desired value. However, if one wants to take full advantage of the exceptional resolution in a DLD device, reasonably close is not always good enough. This highlights, we believe, the need for devices that either have multiple D_{c0} or that are tuneable.

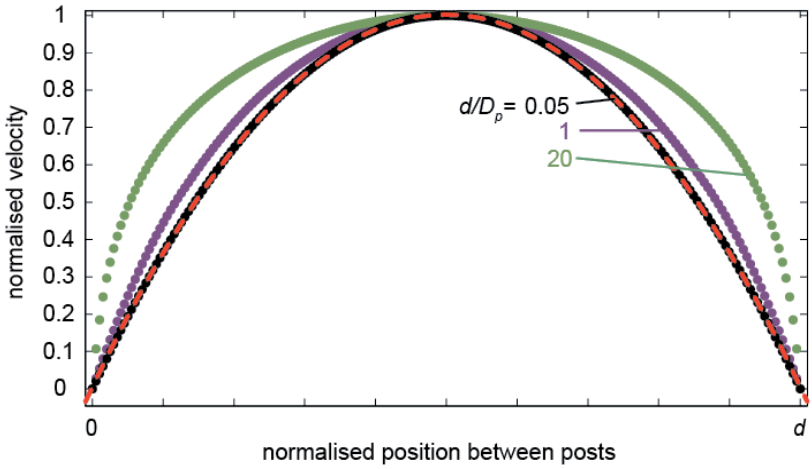

Figure 4.5. Flow profile as a function of the ratio of post diameter and gap size, d/D_{post}. The red dashed line is a parabola.

5 Paper I – Tuneable Separation in Elastomeric Microfluidic Devices

Paper I presents a proof-of-concept for a tuneable DLD device. The basic idea is that a DLD device, fabricated in PDMS, an elastomeric polymer, can be deformed and that this deformation will change *d,* the gap size between the posts, thereby changing the critical size (see Eq. 22). Stretching, squeezing, bending or shearing the block of PDMS containing the DLD array are ways by which stress can be applied and will result in a strain, or in other words a change in the geometry of the array. We choose to create strain in a device by stretching it. Chapter 5.2 will describe how this stretching is achieved and 5.3 will present the results from Paper I but first, in chapter 5.1, we will review, briefly, some of the uses to which the elastomeric properties of PDMS have been put.

5.1 Some uses of PDMS as an elastomer

PDMS is widely used to fabricate microfluidics devices as described by Xia *et al.* [43](see Appendix 2 for a description of the fabrication process, replica moulding, most commonly used to create fluidics devices). PDMS is cheap, biocompatible, compatible with optical microscopy in the wavelength range relevant for most fluorescent molecules and, most importantly in the context of paper I, it is an elastomer. The elastomeric properties of PDMS have been widely exploited in the microfluidics field, both for fabrication purposes and to achieve functionality in actual devices. Soft lithography is regularly done using PDMS stamps [43-45]. Yu *et al.* recently fabricated masters for replica moulding that could be inflated using gas pressure and were able to change the size and curvature of the resultant channels [46]. Various microfluidic components such as valves and pumps are made possible in multilayer devices [47]. Accelerometers [48], optical devices that use the deformability of PDMS to achieve tuneability [49-51] and stretchable electronics [52, 53] have also been reported. Deformable pillars and cantilevers in PDMS have been used to measure the forces that cells generate [54, 55] and a variety of other devices have been developed in which mechanical studies can be performed on cells [56-59]. In some cases the deformability of PDMS can be a limiting factor, high/low aspect ratios [43] or high pressures [60] can limit performance and should be considered at the design stage.

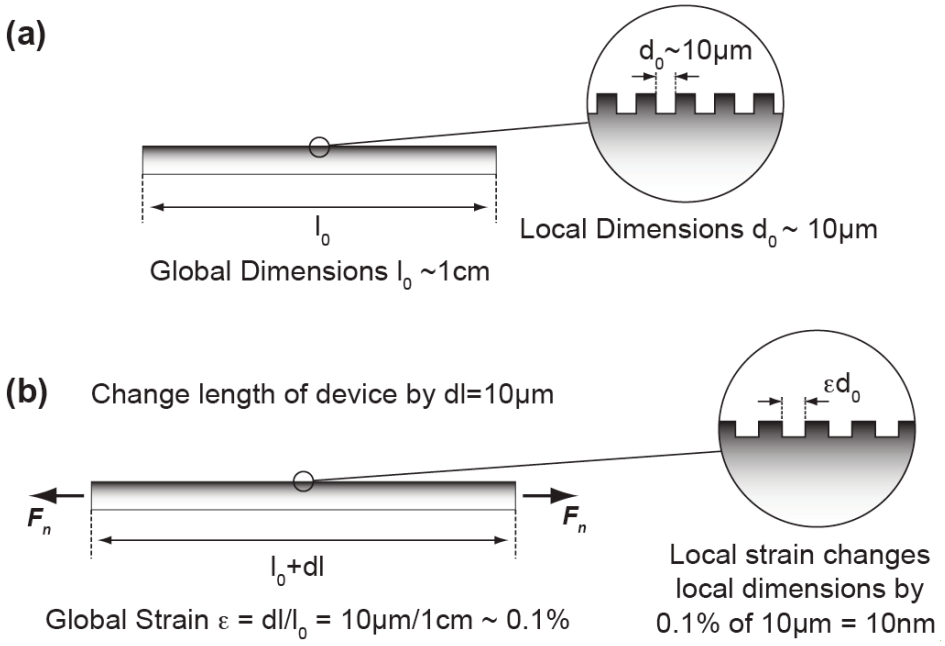

Figure 5.1 Deformation of an elastomer occurs at all scales. (a) The global dimensions of the device can be several centimetres and the local feature size is most often ~10μm. (b) If a global strain is applied then it gives rise to an equal local strain. Global strains of 0.1% are easy to achieve by stretching a device. This relates to a change in local dimensions of ~10nm.

5.2 Stress/Strain – Changing array geometries

What happens when we stretch a piece of PDMS? If a force, F_n, is applied normally to one face of a block of PDMS, with cross sectional area A, then (if the opposite face is fixed) the stress, σ, can be defined as:

$$\sigma = \frac{F_n}{A}. \tag{23}$$

This stress will give rise to an elongation *dl* of the PDMS block. If the initial length of the block was l_0 then we can define a strain ε as:

$$\varepsilon \equiv \frac{dl}{l_0} = \frac{\sigma}{E}. \tag{24}$$

Where E is Young's modulus. The strain generated globally by stretching the entire block of PDMS is mirrored on all scales as depicted in Fig 5.1. Using the setup shown in Fig 5.2, for example, it is relatively easy to change the length of a ~1cm long device by ~10μm. This gives a strain of $\varepsilon = dl/l = 10 \cdot 10^{-6}/10^{-2} = 0.1\%$. In an array where the posts are ~10μm apart this relates to a change in the inter-post distance d of ~0.1%·10μm~10nm. In this way we achieve an adjustable DLD device in which the critical size can be finely tuned.

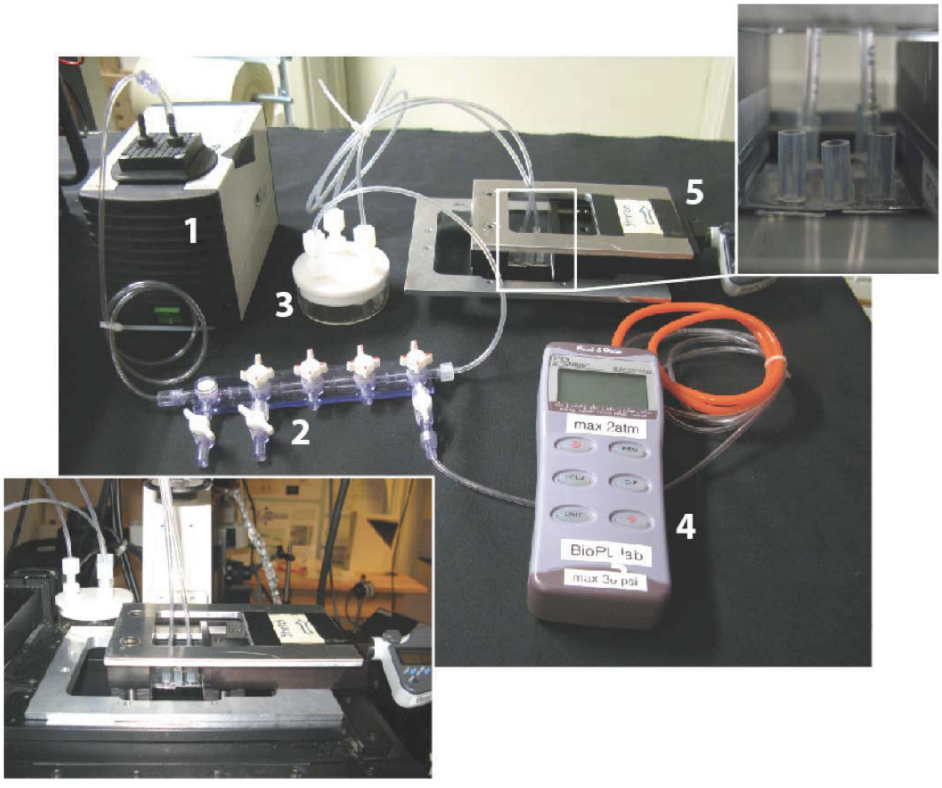

Figure 5.2. The experimental setup for the elastic DLD experiments reported in paper I. Pressure driven flow was created in the device using a vacuum pump (1). The pressure from the pump was controlled using a controlled leak valve (2) and stabilized using a glass bottle as a capacitance (3). The bottle served also to collect waste. Pressure was measured with a pressure gauge (4). The PDMS device was stretched using a custom built chuck (5). The small inset shows the device with fluidic connections mounted in the chuck. The large inset shows the stretching chuck and device mounted in an epifluorescence microscope.

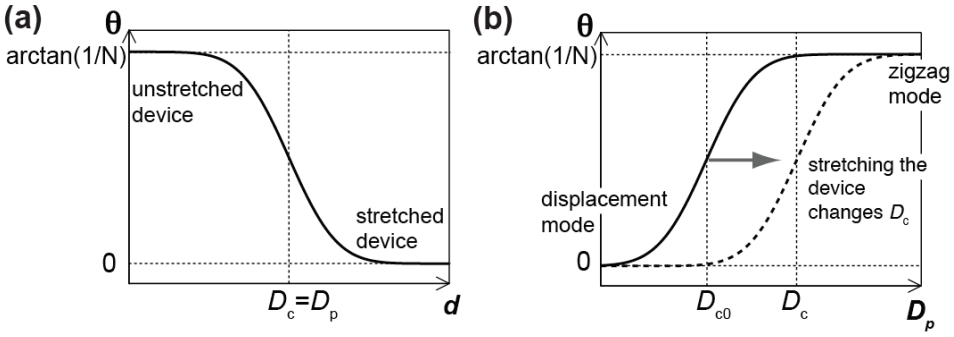

Figure 5.3. The effect stretching has on the behaviour of particles in a DLD device. (a) The trajectory of a monodisperse population of beads with diameter D_p in a device with $D_{c0} < D_p$. As d and therefore D_c is increased the beads make the transition from the displacement mode to the zigzag mode. At the inflection point the critical size is equal to the size of the beads. (b) The trajectory of beads in a device as a function of particle size. Stretching moves the curve, making it possible to choose D_c to suit the system one wishes to separate.

Fig. 5.3 shows how stretching a DLD device with D_{c0} affects the trajectories of beads. 5.3a shows schematically how a monodisperse population of particles with diameter $D_p > D_{c0}$ will move in the displacement mode in an unstretched device. As the device is stretched the gap between the posts, d, increases as does D_c. After sufficient stretching all of the particles will be moving in the zigzag mode. This makes it possible to scan across a population of particles and to determine their size. If the population is not monodisperse† at $D_c > D_p$ the particles will be separated about their mean size. As the width of the transition $\sigma_{total} = (\sigma^2_{bead\ diameter} + \sigma^2_{device})^{0.5}$, once σ_{device} is known the distribution for a non-monodisperse particle population can be determined. It is also possible to stretch and unstretch the device rapidly, in effect creating a switch that turns displacement effects on and off. Fig. 5.3b illustrates how the curve of the displacement angle as a function of particle size can be shifted by stretching.

Note about Poisson's ratio: Poisson's ratio, γ, is the ratio of the transverse strain, or the contraction of the material perpendicular to the applied stress, to the axial strain, or the extension of the material in the direction of the applied stress, $\gamma = \varepsilon_{trans}/\varepsilon_{axial}$. PDMS is an ideal elastic material and has a Poisson's ratio of 0.5. This means that the volume does not change under deformation and that for stretching in the x direction $dl_y/l_{y0} = dl_z/l_{z0} = -0.5 \cdot dl_x/l_{x0}$. This means that as the device is stretched such that d increases

† Note that even truly monodisperse particles in a perfect device would switch randomly between both modes due to diffusion.

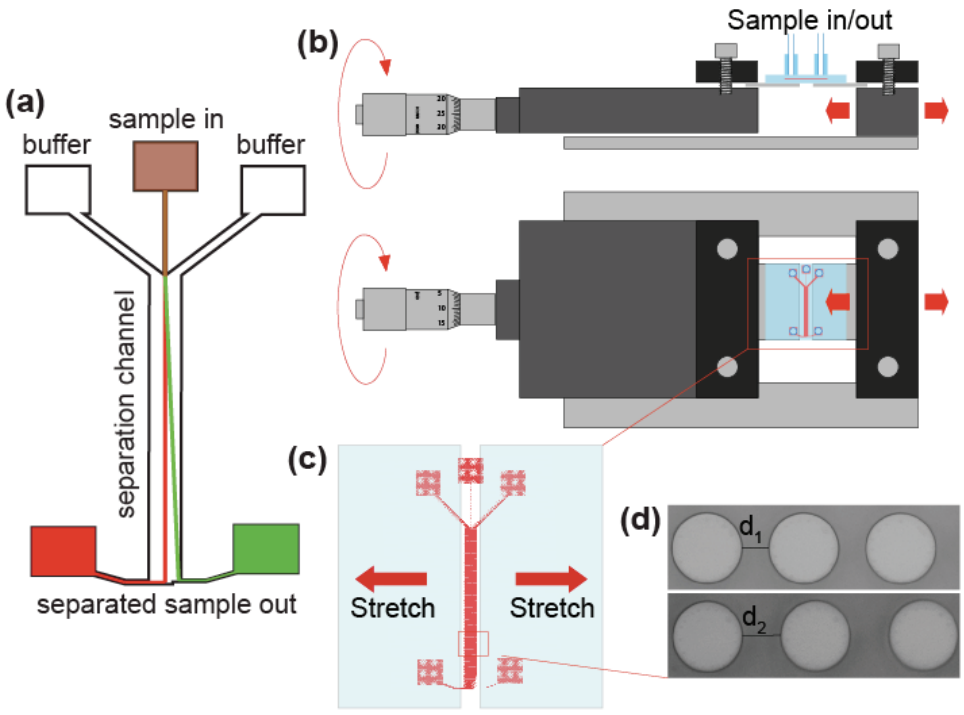

Figure 5.4 Stretching an elastic DLD device to tune the critical size. (a) The sample to be separated is injected into the central channel and focused using a flow of buffer from either side. The inlets are placed to the sides to enable the lateral stretching of the device. (b) The device is mounted in the stretcher chuck, which is in turn mounted in a microscope. This is a schematic of the actual device shown in Fig. 5.2. (c) As stress is applied to the device the array is deformed. (d) The inter-post distance d can be controlled.

the distance between the rows and the depth of the device will decrease. As far as the distance between rows is concerned it has no effect on D_{c0}. However this effect will change the angle $\theta = \arctan(\Delta\lambda/\lambda)$ (see Fig 4.1) and should be considered. This transverse contraction will also affect the depth of the channels and should be taken into account if particles are not to become trapped in shallow devices.

5.3 Results from paper I

Paper I shows how it is possible to tune a DLD device, scanning across a population of polystyrene beads with a mean diameter of 16μm and a coefficient of variation (COV) of 10%†, and how separation of the 16μm beads from 10μm beads can be switched on and off.

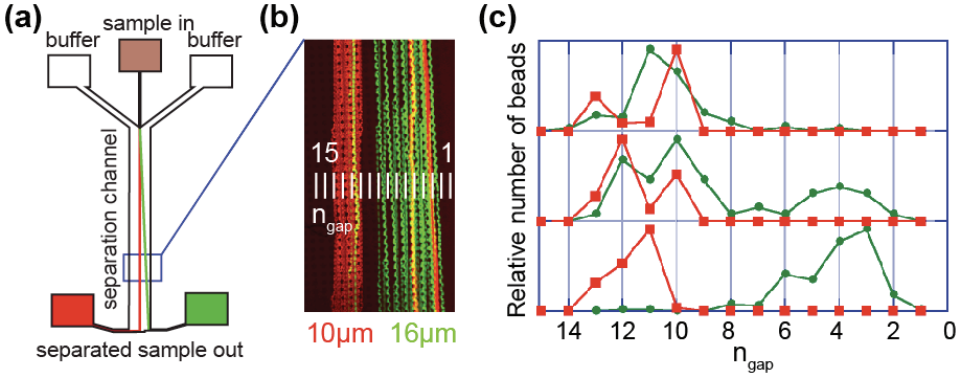

Figure 5.5 Tuning of the critical diameter in the range 10-20μm (a) Separation between posts in this device is 54μm giving a critical diameter D_{c0} of ~13.5μm. (b) A colour enhanced micrograph showing 10μm beads in the zigzag mode and 16μm beads in green in the displacement mode. The gaps between posts are numbered, n_{gap}, and the number of beads passing through each gap counted. (c) The behaviour of the beads at 3 different degrees of stretching. At the top there is no separation, in the middle the 16μm beads are separated into two populations and at the bottom the 10μm and 16μm beads are completely separated.

The method employed to analyse how D_c can be changed as a function of stretching is based on noting the positions of polystyrene beads at a fixed distance along the array (see Fig. 5.5a) as the array is stretched. Fig. 5.5b shows the behaviour of 10μm and 16μm polystyrene beads in a device with D_{c0}=13.5μm with no strain. The gaps between posts are numbered from the sidewall towards the middle of the device as shown in Fig. 5.5b. Beads passing through gap 11 are in the zigzag mode and those passing through gap 4 are in the displacement mode. This method of analysing the trajectories of the beads means that we do not have to worry about the change of the angle θ due to stretching (see the note about Poisson's ratio in the previous section). The number of beads per gap as a function of gap number n_{gap} is shown in Fig. 5.5c for three different strains. In the bottom graph D_c is in the range 10μm<D_c<16μm and beads with a diameter,

† The standard deviation in size as a percentage of the mean size.

D=16μm (shown in green) are separated completely from beads with a diameter, D=10μm (shown in red). In the middle graph D_c has been increased to ~16μm and the 16μm beads are divided into two subpopulations. In the top graph D_c has been further increased to above 16μm and the 16μm and 10μm beads are no longer separated.
The small slope for the 10μm beads (the average gap changes from gap number 12 to gap number 11) is unexpected and most likely due to deformation of the inlet channels or a blockage causing a slight change in the flow pattern as the beads enter the post array area.

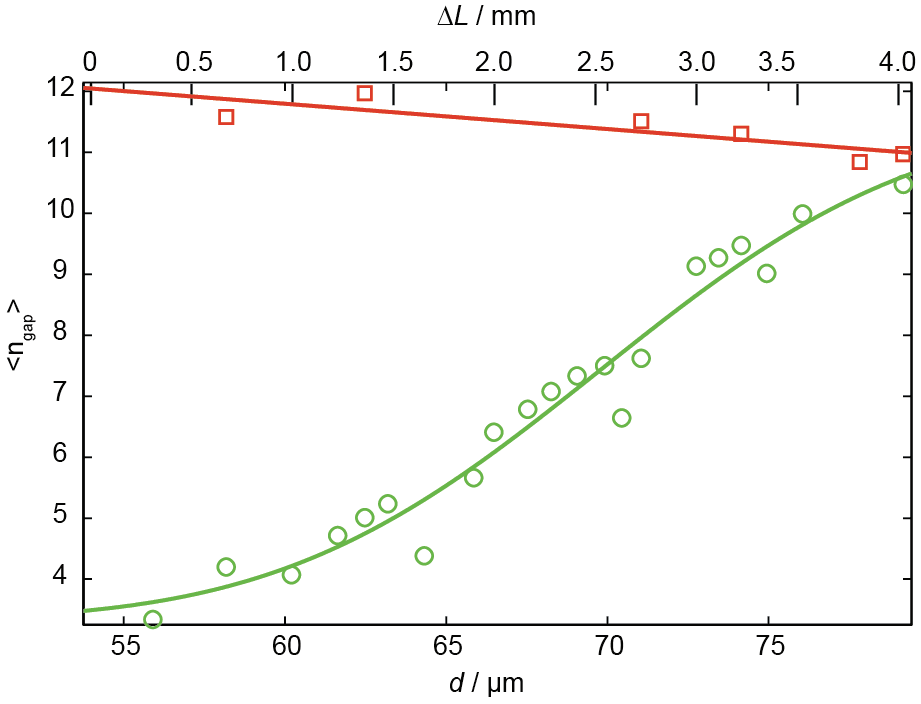

Figure 5.6 The average gap number through which ~100 beads per data point pass as a function of the amount by which the device is stretched and the inter-post distance, d, that this relates to. d values are calculated by measuring the width of the array and dividing by the number of gaps. Red squares show D=10μm beads unaffected by the applied changes in d whereas D=16μm beads, shown in green circles, experience a transition from being displaced by the post array to following the fluid-flow. The red line is a linear fit and the green line is a fit to Eq. 25.

$$\left\langle n_{gap} \right\rangle = \frac{1}{2} n_0 \left(1 + erf\left(\frac{d - d_0}{\sqrt{2\sigma_{total}}} \right) \right) + \frac{1}{2} n_1 \left(1 - erf\left(\frac{d - d_0}{\sqrt{2\sigma_{total}}} \right) \right) \qquad (25)$$

The fit of Eq. 25 to the data in Fig. 5.6 was used together with Eq. 22 to calculate the correction factor α. Using the fact that at the inflection point $D_c = D_p$ = 16μm we obtained, $\alpha = ND_c/2d = 20*16[\mu m]/2*69.77 \pm 3.0\ [\mu m]$ = 2.29 *± 0.1*. This value can be compared to the theoretical value in Fig. 4.4a.

Lastly, using σ_{total} = 6.1μm from the fit we obtain $\sigma_{bead\ diameter}$ = 1.4μm, which is 9% of the mean size of the beads. From this we conclude that the broadening due to the device σ_{device} << 9%.

6 Paper II – Tipping the Balance with Dielectrophoresis – Electrical Deterministic Lateral Displacement Devices

Rather than changing the geometry of a device in order to achieve tuneability as described in the previous chapter, Paper II describes how it can be done by applying an AC field along a DLD device. The electric field lines in the device are forced closer together between the insulating posts and the result is a local gradient in the field that causes polarisable particles to experience DEP as described in chapter 3.3. These forces cause small perturbations in the trajectories of particles as they move past the posts that become magnified by the mechanism of DLD allowing us to combine the sharp cut-off inherent to DLD with the ease of tuneability and versatility of DEP. Importantly, this DEP force is sensitive to many particle parameters other than size and can therefore be leveraged together with DLD for the separation of particles that may have the same size but otherwise be very different. Examples of such particle pairs may be healthy/infected cells or live/dead bacteria.

DEP has been used in a variety of particle manipulation techniques, which we will review briefly in chapter 6.1. Chapter 6.2 will describe how we implement DEP in a DLD device and 6.3 will show some results from paper II.

6.1 DEP to manipulate particles

Since Pohl's first particle manipulations using DEP in the 1960s [34-37], the technique has developed in two main directions. Non-uniform electric fields have been generated in two ways, either using the geometries of electrodes or by modifying the field using insulators. Electrode-based DEP has been used to separate cells using DEP migration where cells with different DEP mobilities migrate to different parts of an electrode array [37, 61], DEP affinity (or retention) where one type of cell is trapped on an electrode array while the other cells are flushed through the device [62] and DEP field flow fractionation (DEP FFF) where cells with differing DEP properties travel at different heights above an electrode array and are therefore eluted at different times due to the parabolic velocity profile [63, 64]. While these methods have been used to trap, separate and analyze a variety of biological

and non-biological particles, they have in common the fact that they only deal with samples one batch at a time.

Among the continuous methods that have been developed using DEP forces are Travelling Wave DEP (TWDEP) where a nonuniform travelling electric field creates a DEP force perpendicular to a planar 2D electrode array [62, 65, 66] and Isomotive Nonuniform Field DEP where the electrodes in a planar 2D array parallel with the flow direction are individually addressed and a resistive ladder is used to create a field gradient perpendicular to the flow direction [67, 68]. DEP forces have also been used for the barriers needed to focus and switch particles in microchip-based flow cytometers [68-71].

Electrodeless or insulator-based DEP (I-DEP) is based on the ability of insulating obstacles, placed between electrodes, to deform the electric field. The insulator-based approach has several advantages when compared to electrode-based methods. Complex channels with insulating constrictions can easily be fabricated in PDMS using soft lithography [43] or alternatively in thermoplastics using imprint-lithography [72] or injection moulding [73]. While these same steps are used to fabricate the channels for electrode-based methods the integration of electrode arrays requires additional fabrication steps. Electrodes are prone to fouling and running electrodes at low frequencies can cause electrolysis, which can affect buffer composition and pH, degrade electrodes and lead to bubble formation, which for microfluidic systems can be detrimental. Insulator-based methods make it possible to position electrodes in reservoirs at the ends of the device or to position integrated electrodes [74] well away from microchannels and structures where bubbles can cause problems and these devices can therefore be run at low frequency and even at DC. While the correct choice of electrode configuration can create extremely high field gradients these gradients are localized near to the surface of the electrodes and DEP forces fall off quickly in the channel above the electrodes. However, the electric field in an insulating constriction is modulated through the entire depth of the channel, perpendicular to the direction of constriction.

The first instances of insulator-based DEP entailed the trapping of particles in constrictions. Masuda *et al.* [75] trapped cell pairs for fusion experiments in an insulating constriction between two electrodes and Chou *et al.* [76] trapped single and double stranded DNA in an array of constrictions. More recently continuous methods, based on DC fields, have been developed in which particles are driven through devices using electrophoresis and electroosmosis and in which DEP forces cause particles to alter their trajectories relative to the carrier fluid. Hawkins *et al.* used an insulating barrier to separate a flow of particles into a continuous distribution of dielectric mobilities perpendicular to the flow direction [77]. Kang *et al.* used a channel with one single obstacle to create a nonuniform electric field [78, 79]. Micrometer sized particles that were driven both

electrophoretically and electroosmotically experienced negative DEP and were caused to move perpendicularly to the fluid flow away from the obstacle, a mechanism that lead to size separation. Lapizco-Encinas *et al.* used DC fields in post arrays to separate live and dead bacteria [80, 81]. The bacteria where driven electrophoretically through the array and became selectively trapped by DEP forces as the voltage was increased. At voltages below the trapping threshold particles where focused in the rows between the posts, an effect which the authors referred to as "streaming dielectrophoresis". Cummings proposed using this effect for the continuous separation of particles [82] by tilting the array with respect to the flow and discussed the effects of post shape and array geometry.

Our method differs from that of Cummings on several important points, as discussed in paper II. Briefly, no effects related to DLD where explored by Cummings. Because the electric field and therefore the electrophoretic effects sum to zero, our use of AC fields allows us to use frequency to tune DEP forces independently of first order electrokinetic effects such as flow rates and global particle velocities.

6.2 Combining DEP and DLD

Fig. 6.1 shows how nDEP† forces can be generated in a post array and how they act to change the critical size in a DLD device. Fig. 6.1a shows a simulation of the electric field in an array performed with COMSOL Multiphysics® 3.4 (COMSOL AB, Stockholm, Sweden)‡. The field is deformed by the insulating posts leading to areas of high (red) and low (blue) field strengths. Fig 6.1b shows the potential energy for a polystyrene bead of diameter 4μm with a Clausius-Mossotti factor of -0.49 calculated using the electric field in Fig. 6.1a and Eq. 9. The black arrows show the direction and magnitude of the DEP force calculated using Eq. 10.

† pDEP forces could also be used but have not as yet been explored. The current discussion is therefore limited to nDEP.

‡ Details of the simulations are to be found in Paper II and the corresponding supporting information.

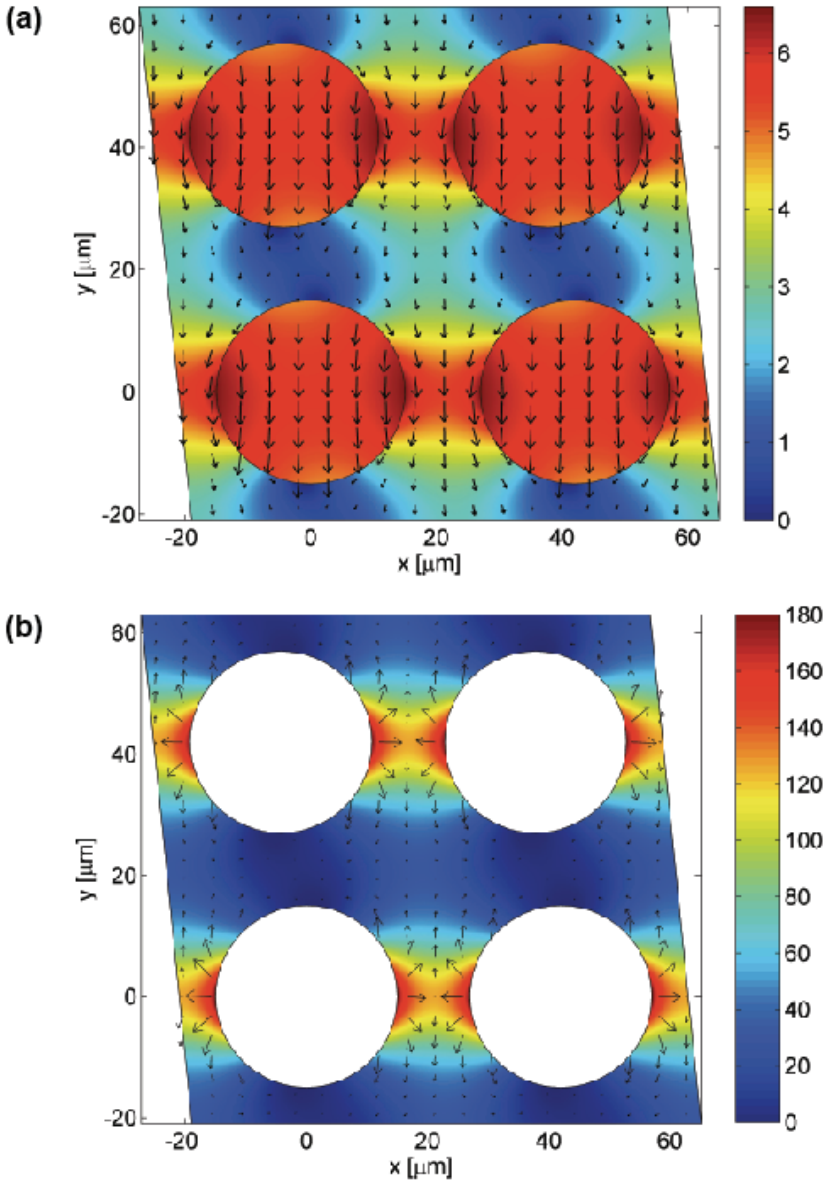

Figure 6.1. Simulations of electric field and potential energy of dielectric beads in a DLD device. (a) Simulation (COMSOL Multiphysics® 3.4 (COMSOL AB, Stockholm, Sweden)) of the electric field in a DLD device. (b) The potential energy for 4μm beads experiencing negative dielectrophoresis. The arrows indicate the direction of F_{DEP}.

The basic mechanism of separation in a device at zero electric field is depicted in Fig. 6.2a. The small bead, shown in red, is in the zigzag mode and

the large bead, shown in green, is in the displacement mode. As an electric field is applied along the device the beads start to experience a force out from the surface of the post as they pass by as shown in Fig. 6.1b. Fig. 6.2b illustrates how, at sufficiently large field strengths, the small bead, which is smaller than D_{c0} in the device, is pushed far enough out from the surface of the post that it will cross into the lamina at P_2 (see chapter 4 for a discussion of the displacement mechanism). Tuneability is gained via control of the DEP force, which is in turn controlled by the applied voltage.

Fig. 6.3 shows the setup that was built to control fluid injection, pressure and applied electric field. The DLD device that was used had a D_{c0} of 6μm and the particles that where studied had diameters of 2, 3, 5 and 10μm. These beads where chosen because they coincide in size with many of the cell types that we have an interest in separating (see table 1.1).

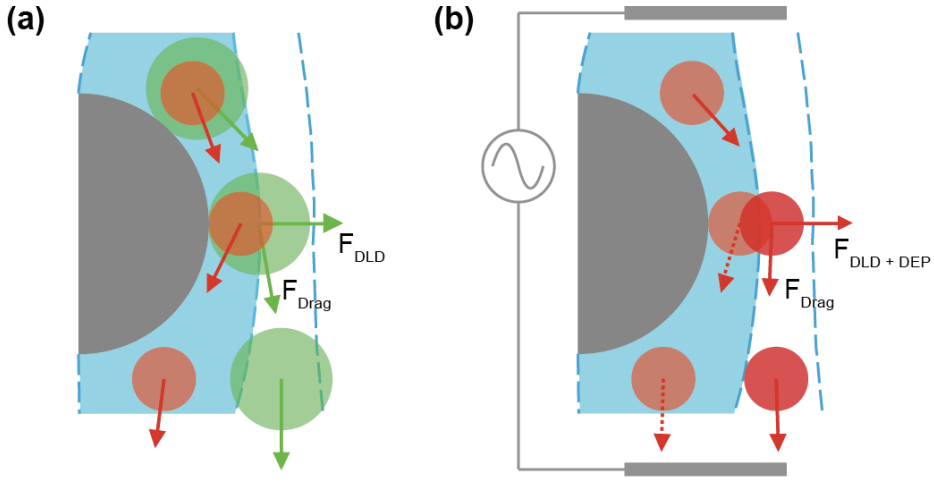

Figure 6.2. Changing the critical size in a DLD device using DEP. (a) At zero field strength the red bead is in the zigzag mode and the green bead is in the displacement mode. (b) When an AC field of sufficient magnitude is applied, F_{DEP} forces the red bead to change flow lanes. The critical size in the device is thus tuned.

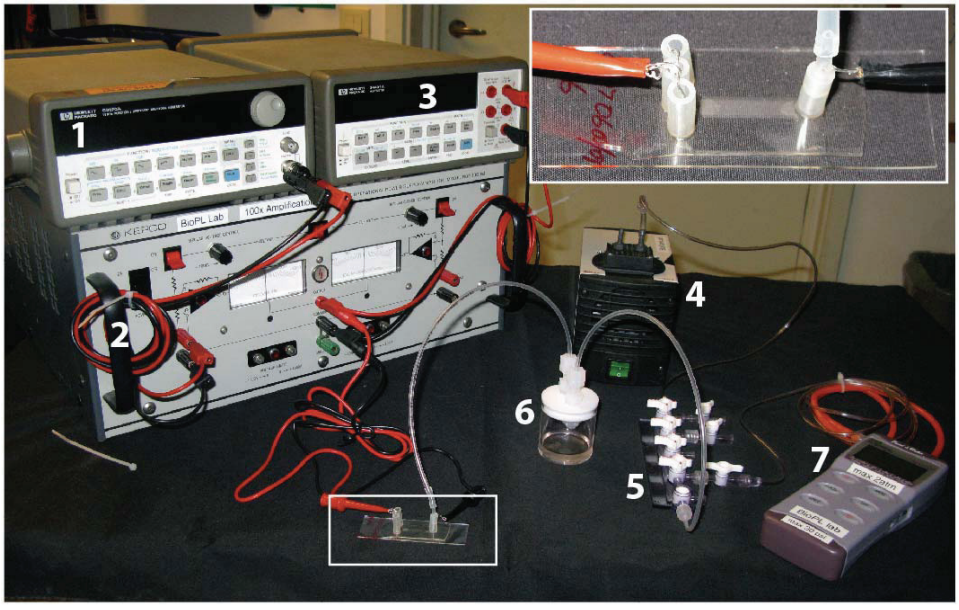

Figure 6.3. The experimental setup for the DEP DLD experiments performed in paper II. The AC voltage was generated with a function generator (1) with a maximum peak-to-peak voltage of 10 V. This signal was then amplified 100x (2) and the resulting voltage measured with a voltmeter (3). Pressure-driven flow was created in the device using a vacuum pump (4). The pressure from the pump was controlled using a controlled leak (5) and stabilized using a glass bottle as a capacitance (6). The bottle served also to collect waste. Pressure was measured with a pressure gauge (7). The inset shows the device with fluidic connections and platinum electrodes.

6.3 Results from paper II

Fig. 6.4a shows how a mixture of beads with D_p = 3µm and 5µm is continuously and completely separated in an array with D_{c0} = 6 µm. A focused stream of beads is injected into the device and kept focused using a sheath flow of buffer on each side. At zero applied field, with $D_p < D_{c0}$ for both bead sizes, all beads are in the displacement mode and no separation occurs (see Fig. 6.4b). Applying an AC voltage of 265 V_{RMS} cm^{-1}† at 100 Hz over the channel reduces D_c such that the 5 µm and 3 µm beads are completely separated (see Fig. 6.4c).

† All voltages stated as V_{RMS} denote the applied RMS voltage/Length of device.

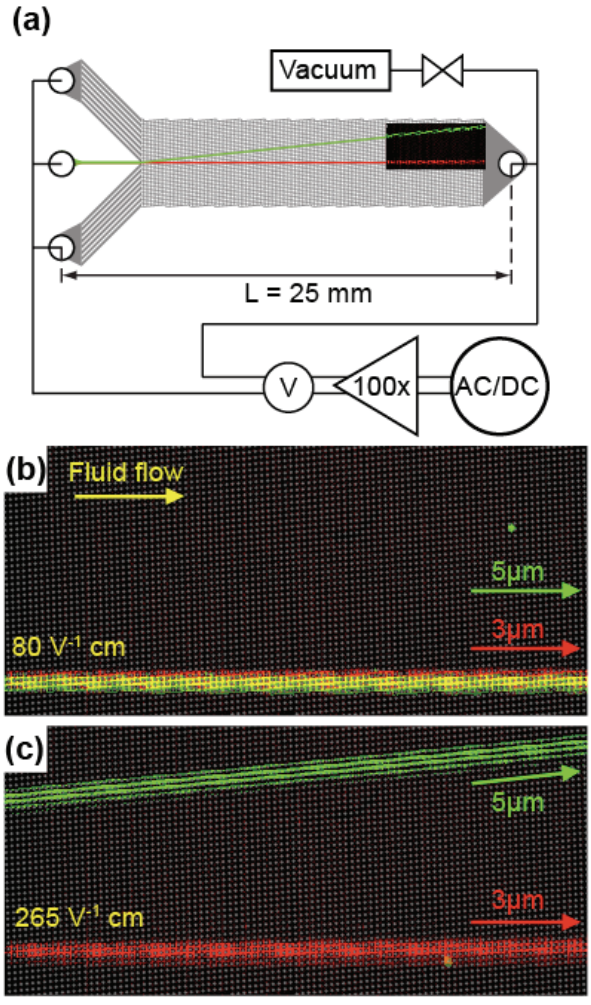

Figure 6.4. Micrograph taken at two wavelengths and averaged over 500 frames of 3 μm (red) and 5 μm (green) diameter polystyrene beads moving with the pressure-driven flow from left to right through a device with D_{c0} = 6 μm shown relative to the device and fluidic and electric connections. (b) In this case the beads are hydrodynamically focused into a stream of approximately 200 μm in width. An AC field at 100 Hz with a magnitude as high as 80 V_{RMS} cm^{-1} has no effect on the trajectories of the particles. The grey overlay highlights the location of the posts. (c) Same as previous image but at 265 V_{RMS} cm^{-1} 3 μm < D_c < 5 μm and the 5 μm beads have therefore made the transition from the zigzag mode to the displacement mode (from movie m1.mov, see ESI – Paper II).

Fig. 6.5a shows the displacement angle for a single particle size as a function of the electric field and defines important parameters such as the critical electric field E_c at which displacement occurs for a specific bead size. The electric field can be used to scan across the distribution in the same way stretching was used in the elastic DLD device in Paper I. Again, in a similar manner to the elastic device, Fig. 6.5b shows how the curve for the displacement angle as a function of bead diameter is shifted when an AC field is applied. Fig. 6.5c shows the mean displacement angle of beads with D_p = 2,3,5 and 10μm as a function of average electric field. The experimental trajectories are measured using a particle tracking program[†]. 10 μm beads (cyan inverted triangles) are in the displacement mode even at 0 V cm^{-1} being larger than the D_{c0}. From 120 V_{RMS} cm^{-1} to 240 V_{RMS} cm^{-1} the 5 μm beads (red circles) make the transition from zigzag to displacement mode. In the interval from 240 V_{RMS} cm^{-1} to 280 V_{RMS} cm^{-1} the 5 μm beads move completely in the displacement mode while the 3 μm beads (green squares) are following the flow, meaning that the critical size in the array has been placed between 3 and 5 μm. At 280 V_{RMS} cm^{-1} to 320 V_{RMS} cm^{-1} the 3 μm beads start to make the transition to the displacement mode and become separated from the 2 μm beads (blue triangles). The dashed lines in Fig. 6.5c show values obtained from simulations of particles with effective diameters corresponding to the actual bead sizes used[‡].

[†] Written in MATLAB® 2007b (The MathWorks™, Natick, MA, USA), full details of which can be found in the appended ESI for Paper II

[‡] A discussion of the simulations is to be found in Paper II and appended ESI. Basically the critical size in the simplified 2D simulation differed slightly from the actual device and so simulated bead sizes were scaled accordingly.

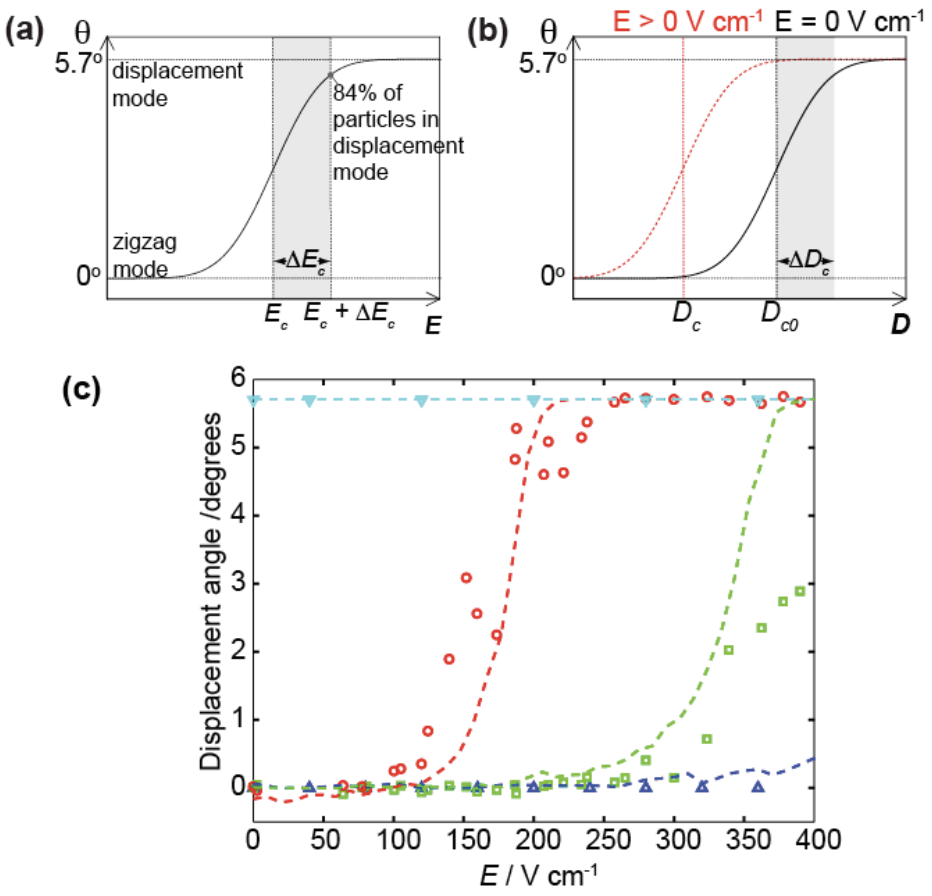

Figure 6.5. Definitions of critical parameters E_c and D_c. At $E_c \pm \Delta E_c$ and $D_c \pm \Delta D_c$ 84%, (erf(1)=0.84), of the particles are in the displacement mode or the zigzag mode respectively. (a) E_c is defined as the electric field strength at which a specific bead size coincides with the critical diameter D_c in the device. (b) D_{c0} and D_c are defined in this plot of bead angular trajectory as a function of bead diameter at zero applied electric field (D_{c0}) and for a positive applied field (D_c). (c) Experimental results. 10 μm diameter beads (cyan triangles) being larger than D_{c0} move in the displacement mode even at 0 V_{RMS} cm^{-1}. 5 μm and 3 μm beads (red circles and green squares respectively) are switched from zigzag mode to displacement mode as the average field and thus the DEP force is increased. 2 μm beads (blue triangles) remain in the zigzag mode but are expected to switch to displacement mode at higher E. The particle velocities are 190 μm s^{-1} at 0 V_{RMS}. The dashed lines are simulated values for the same effective diameter, D_{eff}, as in the experiments. According to the simulations the 2 μm beads should switch over to the displacement mode at 520 V_{RMS} cm^{-1}.

7 Conclusions and Outlook

We have, in this thesis, discussed the benefits of tuneability in particle-particle separation devices and shown how tuneability in DLD devices can be achieved, namely using elastic deformation or the addition of forces to perturb particle trajectories, in this case DEP forces.

The ability to tune the cutoff during separation adds versatility to the method of DLD developed by Huang *et al.* allowing not only fine adjustment, relaxing the strict fabrication requirements, but also new modes of operation of these types of devices.

While further work is needed to address questions related to device performance, much of our efforts will be focused on putting these devices to work, separating biologically relevant particles. The introduction of DEP to DLD, for example, opens up for sorting based not only on size but also on dielectric properties of the particles of interest without the need to perform labelling. Moreover, the exact dielectric features of interest can be selected by choosing a corresponding frequency or combination of frequencies[83]. Another alternative is to first sort particles with regards to size in an array with no applied field and then by $\mathrm{Re}(f_{\mathrm{CM}})$ in a second array, tuned using an AC field. Because the sensitivity of the DEP DLD device is optimal for particles closest in size to D_{c0}, both of these approaches will benefit from the ability to change D_{c0} by elastic deformation and so a combination of tuning via elastic deformation and DEP holds considerable promise.

Teixeira-Pinto *et al.* [84] first observed how nonspherical particles adapt specific orientations in an AC field. Miller and Jones later showed how the orientation of nonspherical cells, namely eurythrocytes, in an AC field is frequency dependent [85]. This frequency-dependent orientation could be used to probe the geometry of nonspherical particles in a DLD device and allow the separation of particles of different shape that might otherwise have the same effective size.

Finally, although we chose in paper II to combine DLD with DEP due to its simplicity, in fact it is conceivable to amplify any type of minute force interaction in this way by combination with DLD, such as for example magnetic, gravitational or optical forces[†].

[†] For example a DLD device can be oriented such that gravitational forces tip the balance. Results to be presented at Micro Total Analysis Systems 2009, South Korea.

Appendix 1

List of Acronyms and Notation

μTAS	micro total analysis systems
DLD	deterministic lateral displacement
VLP	virus-like particle
POC	point of care
PDMS	poly(dimethylsiloxane)
DEP	dielectrophoresis
nDEP	negative dielectrophoresis
pDEP	positive dielectrophoresis
I-DEP	insulator-based dielectrophoresis
AC	alternating current
DC	direct current
DNA	deoxyribonucleic acid
Re	Reynolds number
Pe	Péclet number
D_H	hydraulic diameter
W_{DEP}	dielectrophoretic energy
F_{DEP}	dielectrophoretic force
ρ	density
v	velocity
t	time
p	pressure
η	dynamic viscosity
ϕ_{gap}	fluid flux between two posts
ϕ_N	1/N of the fluid flux between two posts
f, **F**	force
m	mass
a	acceleration
l, L	length
a, r	radius
D_{post}	post diameter
D_p	particle diameter
D_c	critical diameter (in a DLD device)
D_{c0}	critical diameter at zero applied field (in a DEP DLD device)
N	period in a DLD device

α.....correction factor
λ.....post spacing (centre to centre)
$\Delta\lambda$.....row shift
x,y,z.....spatial coordinates
ε .....permittivity of free space
ε_m.....permittivity of suspending medium
ε_p.....permittivity of particle
f_{CM}.....Clausius-Mossotti factor
E_{RMS}.....root mean square value of electric field
V_{RMS}.....root mean square voltage
D .....diffusion coefficient
p.....polarization
k_B .....Boltzmann's constant
T.....temperature

Appendix 2

Fabrication of Microfluidic Devices using Replica Moulding

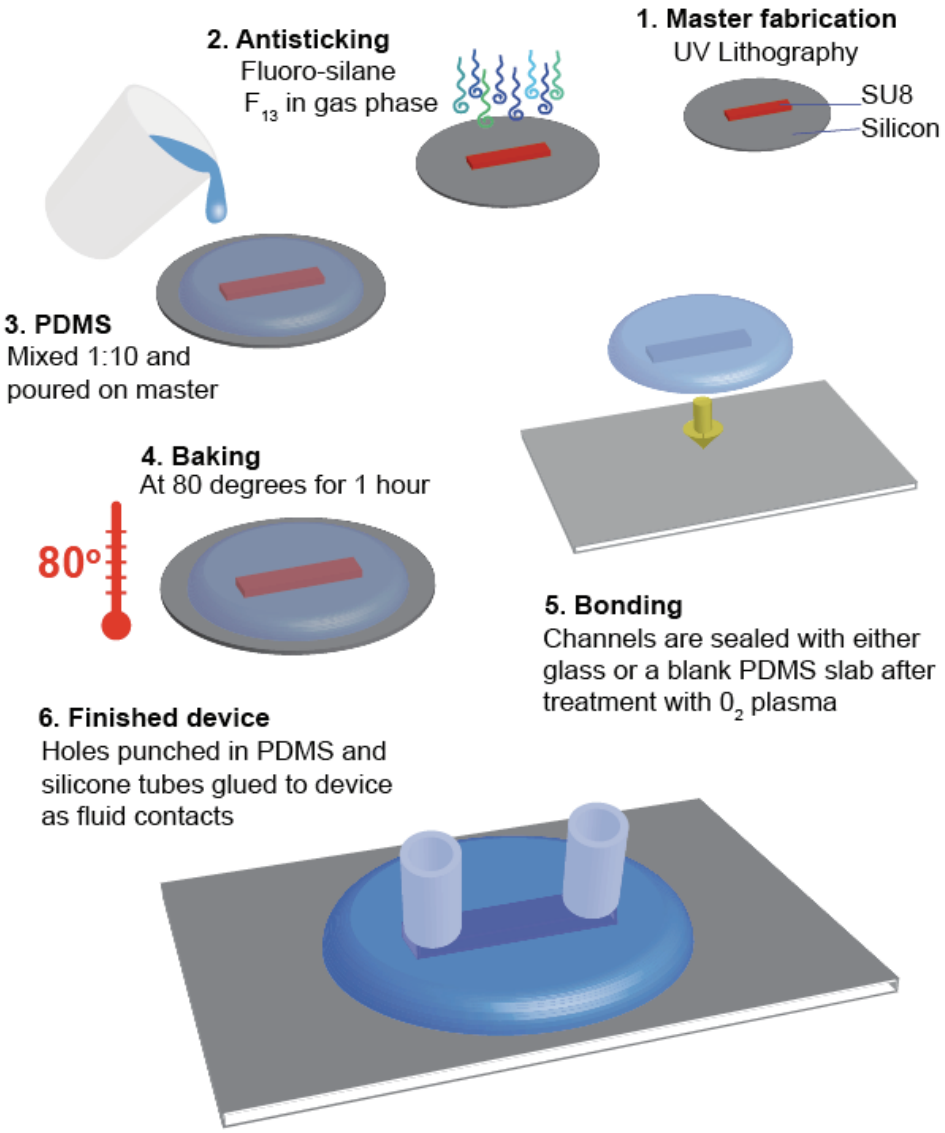

References

1. Huang, L.R., E.C. Cox, R.H. Austin, and J.C. Sturm, *Continuous Particle Separation Through Deterministic Lateral Displacement.* Science, 2004. **304**(5673): p. 987-990.
2. Giddings, J.C., *Unified Separation Science*. 1991, New York: Wiley. xxiv, 320 p.
3. van Hee, P., M.A. Hoeben, R.G.J.M. van der Lans, and L.A.M. van der Wielen, *Strategy for Selection of Methods for Separation of Bioparticles from Particle Mixtures.* Biotechnology and Bioengineering, 2006. **94**(4): p. 689-709.
4. Laerum, O.D. and T. Farsund, *Clinical Application of Flow Cytometry - A Review.* Cytometry, 1981. **2**(1): p. 1-13.
5. Pappas, D. and K. Wang, *Cellular Separations: A Review of New Challenges in Analytical Chemistry.* Analytica Chimica Acta, 2007. **601**(1): p. 26-35.
6. Terry, S.C., J.H. Jerman, and J.B. Angell, *Gas-Chromatographic Air Analyzer Fabricated on a Silicon-Wafer.* Ieee Transactions on Electron Devices, 1979. **26**(12): p. 1880-1886.
7. Manz, A., N. Graber, and H.M. Widmer, *Miniaturized Total Chemical-Analysis Systems - a Novel Concept for Chemical Sensing.* Sensors and Actuators B-Chemical, 1990. **1**(1-6): p. 244-248.
8. Franke, T.A. and A. Wixforth, *Microfluidics for Miniaturized Laboratories on a Chip.* Chemphyschem, 2008. **9**(15): p. 2140-2156.
9. Erickson, D. and D.Q. Li, *Integrated Microfluidic Devices.* Analytica Chimica Acta, 2004. **507**(1): p. 11-26.
10. Verpoorte, E. and N.F. De Rooij, *Microfluidics Meets MEMS.* Proceedings of the Ieee, 2003. **91**(6): p. 930-953.
11. Craighead, H., *Future Lab-On-A-Chip Technologies for Interrogating Individual Molecules.* Nature, 2006. **442**(7101): p. 387-393.
12. Andersson, H. and A. van den Berg, *Microfluidic Devices for Cellomics: A Review.* Sensors and Actuators B-Chemical, 2003. **92**(3): p. 315-325.
13. Chen, X. and D.F. Cui, *Microfluidic Devices for Sample Pretreatment and Applications.* Microsystem Technologies-Micro-and Nanosystems-Information Storage and Processing Systems, 2009. **15**(5): p. 667-676.
14. El-Ali, J., P.K. Sorger, and K.F. Jensen, *Cells on Chips.* Nature, 2006. **442**(7101): p. 403-411.
15. Yager, P., T. Edwards, E. Fu, K. Helton, K. Nelson, M.R. Tam, and B.H. Weigl, *Microfluidic Diagnostic Technologies for Global Public Health.* Nature, 2006. **442**(7101): p. 412-418.
16. Pamme, N., *Continuous Flow Separations in Microfluidic Devices.* Lab on a Chip, 2007. **7**(12): p. 1644-1659.

17. Davis, J.A., D.W. Inglis, K.J. Morton, D.A. Lawrence, L.R. Huang, S.Y. Chou, J.C. Sturm, and R.H. Austin, *Deterministic Hydrodynamics: Taking Blood Apart.* Proceedings of the National Academy of Sciences of the United States of America, 2006. **103**(40): p. 14779-14784.
18. Inglis, D.W., J.A. Davis, T.J. Zieziulewicz, D.A. Lawrence, R.H. Austin, and J.C. Sturm, *Determining Blood Cell Size Using Microfluidic Hydrodynamics.* Journal of Immunological Methods, 2008. **329**(1-2): p. 151-156.
19. Inglis, D.W., K.J. Morton, J.A. Davis, T.J. Zieziulewicz, D.A. Lawrence, R.H. Austin, and J.C. Sturm, *Microfluidic Device for Label-Free Measurement of Platelet Activation.* Lab on a Chip, 2008. **8**(6): p. 925-931.
20. Morton, K.J., J.C. Sturm, R.H. Austin, and S.Y. Chou. *Nanoimprinted Fluidic Device for Continuous Separation of Nanoparticles*. in *10th International Conference on Miniaturized Systems for Chemistry and Life Sciences*, Tokyo, 2006: p. 1014-1016.
21. Morton, K.J., K. Loutherback, D.W. Inglis, O.K. Tsui, J.C. Sturm, S.Y. Chou, and R.H. Austin, *Crossing Microfluidic Streamlines to Lyse, Label and Wash Cells.* lab chip, 2008. **8**(9): p. 1448–1453.
22. Morton, K.J., K. Loutherback, D.W. Inglis, O.K. Tsui, J.C. Sturm, S.Y. Chou, and R.H. Austin, *Hydrodynamic Metamaterials: Microfabricated Arrays to Steer, Refract, and Focus Streams of Biomaterials.* Proceedings of the National Academy of Sciences of the United States of America, 2008. **105**(21): p. 7434-7438.
23. Bruus, H., *Theoretical Microfluidics*. Oxford master series in condensed matter physics 2007: Oxford university press. p. 364.
24. Hauke, G., *An Introduction to Fluid Mechanics and Transport Phenomena*. 2008, New York: Springer. p. 296.
25. Nguyen, N.-T. and S.T. Wereley, *Fundamentals and Applications of Microfluidics*. 2nd ed. Artech House integrated microsystems series. 2006, Boston: Artech House. xiii, 497 p.
26. Di Carlo, D., J.F. Edd, D. Irimia, R.G. Tompkins, and M. Toner, *Equilibrium Separation and Filtration of Particles Using Differential Inertial Focusing.* Analytical Chemistry, 2008. **80**(6): p. 2204-2211.
27. Di Carlo, D., D. Irimia, R.G. Tompkins, and M. Toner, *Continuous Inertial Focusing, Ordering, and Separation of Particles in Microchannels.* Proceedings of the National Academy of Sciences of the United States of America, 2007. **104**(48): p. 18892-18897.
28. Brody, J.P., T.D. Osborn, F.K. Forster, and P. Yager, *A Planar Microfabricated Fluid Filter.* Sensors and Actuators a-Physical, 1996. **54**(1-3): p. 704-708.

29. Ji, H.M., V. Samper, Y. Chen, C.K. Heng, T.M. Lim, and L. Yobas, *Silicon-Based Microfilters for Whole Blood Cell Separation.* Biomedical Microdevices, 2008. **10**(2): p. 251-257.
30. Lay, C., C.Y. Teo, L. Zhu, X.L. Peh, H.M. Ji, B.R. Chew, R. Murthy, H.H. Feng, and W.T. Liu, *Enhanced Microfiltration Devices Configured with Hydrodynamic Trapping and a Rain Drop Bypass Filtering Architecture for Microbial Cells Detection.* Lab on a Chip, 2008. **8**(5): p. 830-833.
31. Di Carlo, D., L.Y. Wu, and L.P. Lee, *Dynamic Single Cell Culture Array.* Lab on a Chip, 2006. **6**(11): p. 1445-1449.
32. Huebner, A., D. Bratton, G. Whyte, M. Yang, A.J. deMello, C. Abell, and F. Hollfelder, *Static Microdroplet Arrays: A Microfluidic Device for Droplet Trapping, Incubation and Release for Enzymatic and Cell-Based Assays.* Lab on a Chip, 2009. **9**(5): p. 692-698.
33. Yamada, M., M. Nakashima, and M. Seki, *Pinched Flow Fractionation: Continuous Size Separation of Particles Utilizing a Laminar Flow Profile in a Pinched Microchannel.* Analytical Chemistry, 2004. **76**(18): p. 5465-5471.
34. Pohl, H.A., *Dielectrophoresis, a New Technique for Studying Cells and Organelles.* Bulletin of the American Physical Society, 1970. **15**(11): p. 1362-&.
35. Pohl, H.A., *Biological Dielectrophoresis.* Bulletin of the American Physical Society, 1973. **18**(3): p. 320-320.
36. Pohl, H.A. and J.S. Crane, *Dielectrophoresis of Cells.* Biophysical Journal, 1971. **11**(9): p. 711-727.
37. Pohl, H.A. and I. Hawk, *Separation of Living and Dead Cells by Dielectrophoresis.* Science, 1966. **152**(3722): p. 647-649.
38. Morgan, H. and N. Green, *AC Electrokinetics: Colloids and Nanoparticles*. Microtechnologies and microsystems series, ed. P.R. Pethig. 2003: Research Studies Press Ltd. p. 250.
39. Inglis, D.W., *Microfluidic Devices for Cell Separation*, Doctoral Thesis, 2008, Princeton, http://web.science.mq.edu.au/~dinglis/, accessed Aug 2009
40. Inglis, D.W., J.A. Davis, R.H. Austin, and J.C. Sturm, *Critical Particle Size for Fractionation by Deterministic Lateral Displacement.* Lab on a Chip, 2006. **6**(5): p. 655-658.
41. Loutherback, K., J. Puchalla, R.H. Austin, and J.C. Sturm, *Deterministic Microfluidic Ratchet.* Physical Review Letters, 2009. **102**(4): p. 145301.
42. Heller, M. and H. Bruus, *A Theoretical Analysis of the Resolution Due to Diffusion and Size Dispersion of Particles in Deterministic Lateral Displacement Devices.* Journal of Micromechanics and Microengineering, 2008. **18**(7): p. 075030.
43. Xia, Y.N. and G.M. Whitesides, *Soft lithography.* Annual Review of Materials Science, 1998. **28**: p. 153-184.

44. Michel, B., A. Bernard, A. Bietsch, E. Delamarche, M. Geissler, D. Juncker, H. Kind, J.P. Renault, H. Rothuizen, H. Schmid, P. Schmidt-Winkel, R. Stutz, and H. Wolf, *Printing Meets Lithography: Soft Approaches to High-Resolution Printing.* Ibm Journal of Research and Development, 2001. **45**(5): p. 697-719.
45. Whitesides, G.M., E. Ostuni, S. Takayama, X.Y. Jiang, and D.E. Ingber, *Soft Lithography in Biology and Biochemistry.* Annual Review of Biomedical Engineering, 2001. **3**: p. 335-373.
46. Yu, H.B., G.Y. Zhou, C.F. Siong, S.H. Wang, and F.W. Lee, *Novel Polydimethylsiloxane (PDMS) Based Microchannel Fabrication Method for Lab-On-A-Chip Application.* Sensors and Actuators B-Chemical, 2009. **137**(2): p. 754-761.
47. Unger, M.A., H.P. Chou, T. Thorsen, A. Scherer, and S.R. Quake, *Monolithic Microfabricated Valves and Pumps by Multilayer Soft Lithography.* Science, 2000. **288**(5463): p. 113-116.
48. Lotters, J.C., W. Olthuis, P.H. Veltink, and P. Bergveld. *Polydimethylsiloxane as an Elastic Material Applied in a Capacitive Accelerometer*. in *6th European Workshop on Micromechanics (MME 95)*, Copenhagen, Denmark, 1995: p. 52-54.
49. Werber, A. and H. Zappe, *Tunable Pneumatic Microoptics.* Journal of Microelectromechanical Systems, 2008. **17**(5): p. 1218-1227.
50. Park, W. and J.B. Lee, *Mechanically Tunable Photonic Crystal Structure.* Applied Physics Letters, 2004. **85**(21): p. 4845-4847.
51. Li, Z.Y., Z.Y. Zhang, A. Scherer, and D. Psaltis, *Mechanically Tunable Optofluidic Distributed Feedback Dye Laser.* Optics Express, 2006. **14**(22): p. 10494-10499.
52. Gonzalez, M., F. Axisa, F. Bossuyt, Y.Y. Hsu, B. Vandevelde, and J. Vanfleteren, *Design and Performance of Metal Conductors for Stretchable Electronic Circuits.* Circuit World, 2009. **35**(1): p. 22-29.
53. Jones, J., S.P. Lacour, and S. Wagner. *Interconnects for Elastically Stretchable and Deformable Electronic Surfaces*. in *Symposium on Materials, Technology and Reliability of Advanced Interconnects held at the 2005 MRS Spring Meeting*, San Francisco, CA, 2005: p. 399-404.
54. Park, J., J. Ryu, S.K. Choi, E. Seo, J.M. Cha, S. Ryu, J. Kim, B. Kim, and S.H. Lee, *Real-Time Measurement of the Contractile Forces of Self-Organized Cardiomyocytes on Hybrid Biopolymer Microcantilevers.* Analytical Chemistry, 2005. **77**(20): p. 6571-6580.
55. Zhao, Y. and X. Zhang. *In Situ Force Probing for Cardiac Myocyte Using PDMS Pillar Array*. in *8th International Conference on Miniaturized Systems for Chemistry and Life Sciences*, Malmo, SWEDEN, 2004: p. 430-432.

56. Cao, Y., J. Chen, M.O. Adeoye, and W.O. Soboyejo, *Investigation of the Spreading and Adhesion of Human Osteosarcoma Cells on Smooth and Micro-Grooved Polydimethylsiloxane Surfaces.* Materials Science & Engineering C-Biomimetic and Supramolecular Systems, 2009. **29**(1): p. 119-125.
57. Kim, Y.C., S.J. Park, and J.K. Park, *Biomechanical Analysis of Cancerous and Normal Cells Based on Bulge Generation in a Microfluidic Device.* Analyst, 2008. **133**(10): p. 1432-1439.
58. Mehta, G., J. Lee, W. Cha, Y.C. Tung, J.J. Linderman, and S. Takayama, *Hard Top Soft Bottom Microfluidic Devices for Cell Culture and Chemical Analysis.* Analytical Chemistry, 2009. **81**(10): p. 3714-3722.
59. Selby, J.C. and M.A. Shannon, *Inflation of a Circular Elastomeric Membrane into a Horizontally Semi-Infinite Liquid Reservoir of Finite Vertical Depth: Quasi-Static Deformation Model.* International Journal of Engineering Science, 2009. **47**(5-6): p. 700-717.
60. Hardy, B.S., K. Uechi, J. Zhen, and H.P. Kavehpour, *The Deformation of Flexible PDMS Microchannels under a Pressure Driven Flow.* Lab on a Chip, 2009. **9**(7): p. 935-938.
61. Gascoyne, P.R.C., Y. Huang, R. Pethig, J. Vykoukal, and F.F. Becker, *Dielectrophoretic Separation of Mammalian-Cells Studied by Computerized Image-Analysis.* Measurement Science & Technology, 1992. **3**(5): p. 439-445.
62. Becker, F.F., X.B. Wang, Y. Huang, R. Pethig, J. Vykoukal, and P.R.C. Gascoyne, *Separation Of Human Breast-Cancer Cells From Blood By Differential Dielectric Affinity.* Proceedings of the National Academy of Sciences of the United States of America, 1995. **92**(3): p. 860-864.
63. Gascoyne, P.R.C., Y. Huang, X.J. Wang, J. Yang, G. DeGasperis, and X.B. Wang, *Cell Separation by Conventional Dielectrophoresis Combined with Field-Flow-Fractionation.* Biophysical Journal, 1996. **70**(2): p. Tu412-Tu412.
64. Huang, Y., X.B. Wang, F.F. Becker, and P.R.C. Gascoyne, *Introducing Dielectrophoresis as a New Force Field for Field-Flow Fractionation.* Biophysical Journal, 1997. **73**(2): p. 1118-1129.
65. Fuhr, G., R. Hagedorn, T. Muller, W. Benecke, B. Wagner, and J. Gimsa, *Asynchronous Traveling-Wave Induced Linear Motion Of Living Cells.* Studia Biophysica, 1991. **140**(2): p. 79-102.
66. Huang, Y., X.B. Wang, J.A. Tame, and R. Pethig, *Electrokinetic Behavior of Colloidal Particles in Travelling Electric-Fields - Studies Using Yeast Cells.* Journal of Physics D-Applied Physics, 1993. **26**(9): p. 1528-1535.
67. Li, Y.L., C. Dalton, H.J. Crabtree, G. Nilsson, and K.V.I.S. Kaler, *Continuous Dielectrophoretic Cell Separation Microfluidic Device.* Lab on a Chip, 2007. **7**(2): p. 239-248.

68. Fiedler, S., S.G. Shirley, T. Schnelle, and G. Fuhr, *Dielectrophoretic Sorting of Particles and Cells in a Microsystem.* Analytical Chemistry, 1998. **70**(9): p. 1909-1915.
69. Holmes, D., H. Morgan, and N.G. Green, *High throughput particle analysis: Combining dielectrophoretic particle focussing with confocal optical detection.* Biosensors & Bioelectronics, 2006. **21**(8): p. 1621-1630.
70. Yu, C.H., J. Vykoukal, D.M. Vykoukal, J.A. Schwartz, L. Shi, and P.R.C. Gascoyne, *A Three-Dimensional Dielectrophoretic Particle Focusing Channel for Microcytometry Applications.* Journal of Microelectromechanical Systems, 2005. **14**(3): p. 480-487.
71. Hu, X.Y., P.H. Bessette, J.R. Qian, C.D. Meinhart, P.S. Daugherty, and H.T. Soh, *Marker-Specific Sorting of Rare Cells Using Dielectrophoresis.* Proceedings of the National Academy of Sciences of the United States of America, 2005. **102**(44): p. 15757-15761.
72. Chou, S.Y., P.R. Krauss, and P.J. Renstrom, *Imprint of Sub-25 Nm Vias and Trenches in Polymers.* Applied Physics Letters, 1995. **67**(21): p. 3114-3116.
73. Becker, H. and C. Gartner, *Polymer Microfabrication Methods for Microfluidic Analytical Applications.* Electrophoresis, 2000. **21**(1): p. 12-26.
74. Demierre, N., T. Braschler, P. Linderholm, U. Seger, H. van Lintel, and P. Renaud, *Characterization and Optimization of Liquid Electrodes for Lateral Dielectrophoresis.* Lab on a Chip, 2007. **7**(3): p. 355-365.
75. Masuda, S., M. Washizu, and T. Nanba, *Novel Method of Cell-Fusion in Field Constriction Area in Fluid Integrated-Circuit.* Ieee Transactions on Industry Applications, 1989. **25**(4): p. 732-737.
76. Chou, C.F., J.O. Tegenfeldt, O. Bakajin, S.S. Chan, E.C. Cox, N. Darnton, T. Duke, and R.H. Austin, *Electrodeless Dielectrophoresis of Single- and Double-Stranded DNA.* Biophysical Journal, 2002. **83**(4): p. 2170-2179.
77. Hawkins, B.G., A.E. Smith, Y.A. Syed, and B.J. Kirby, *Continuous-Flow Particle Separation by 3D Insulative Dielectrophoresis Using Coherently Shaped, DC-Biased, AC Electric Fields.* Analytical Chemistry, 2007. **79**(19): p. 7291-7300.
78. Kang, K.H., Y.J. Kang, X.C. Xuan, and D.Q. Li, *Continuous separation of microparticies by size with direct current-dielectrophoresis.* Electrophoresis, 2006. **27**(3): p. 694-702.
79. Kang, K.H., X.C. Xuan, Y.J. Kang, and D.Q. Li, *Effects of DC-Dielectrophoretic Force on Particle Trajectories in Microchannels.* Journal of Applied Physics, 2006. **99**(6): p. 064702.
80. Lapizco-Encinas, B.H., R.V. Davalos, B.A. Simmons, E.B. Cummings, and Y. Fintschenko, *An Insulator-Based (Electrodeless) Dielectrophoretic*

Concentrator for Microbes in Water. Journal of Microbiological Methods, 2005. **62**(3): p. 317-326.
81. Lapizco-Encinas, B.H., B.A. Simmons, E.B. Cummings, and Y. Fintschenko, *Dielectrophoretic Concentration and Separation of Live and Dead Bacteria in an Array of Insulators.* Analytical Chemistry, 2004. **76**(6): p. 1571-1579.
82. Cummings, E.B., *Streaming Dielectrophoresis for Continuous-Flow Microfluidic Devices.* IEEE Engineering in Medicine and Biology Magazine, 2003. **22**(6): p. 75-84.
83. Braschler, T., N. Demierre, E. Nascimento, T. Silva, A.G. Oliva, and P. Renaud, *Continuous separation of cells by balanced dielectrophoretic forces at multiple frequencies.* Lab on a Chip, 2008. **8**(2): p. 280-286.
84. Teixeirapinto, A.A., L.L. Nejelski, J.L. Cutler, and J.H. Heller, *The Behavior of Unicellular Organisms in an Electromagnetic Field.* Experimental Cell Research, 1960. **20**(3): p. 548-564.
85. Miller, R.D. and T.B. Jones, *Electro-Orientation of Ellipsoidal Erythrocytes - Theory and Experiment.* Biophysical Journal, 1993. **64**(5): p. 1588-1595.